

Synthesis, Properties and Characterization of Metal Nanoparticles



K. Thummavichai, Y. Chen, N. N. Wang, Y. Q. Zhu, and O. Ola

Abstract Precious metals including Au, Pd, Pt, Ag and Pd and other metals such as Fe, Co, Mg and Ni as solid powder, dispersion in solution and deposition as thin films have attained wide interest in the last decades. They have induced intense research interest in nanotechnology due to their exciting properties including good conductivity, magnetic recording, localized surface plasmon resonance, antibacterial and catalytic effects [1, 2]. This chapter will introduce several main synthesis and characterization methods of metallic nanoparticles (NPs). The unique feature, key parameters and especially advantages and disadvantages of top-down (i.e. physical vapour deposition, ball milling and lithography) and bottom-up (e.g. chemical vapour deposition, sol–gel, hydrothermal/solvothermal, etc.) methodologies are discussed to trigger advances in nanotechnology advancement. Alternative green synthesis approaches are also included in this chapter. Furthermore, the basic characterization techniques for metallic NPs are pointed out for improving synthesis strategies, deciphering the topography evolution and comprehending the potential applications. Finally, emphasis has been placed on some main properties of metallic NPs for the potential of a wide range of applications.

Keywords Metallic nanoparticles · Physicochemical characterization · Nanoparticle synthesis · Properties of metallic nanoparticles

K. Thummavichai

Department of Mathematics, Physics and Electrical Engineering, Northumbria University, Newcastle Upon Tyne, UK

Y. Chen · Y. Q. Zhu

College of Engineering, Mathematics and Physical Sciences, University of Exeter, Exeter, UK

N. N. Wang

Guangxi Institute Fullerene Technology (GIFT), Laboratory of New Processing Technology for Nonferrous Metals and Materials, Ministry of Education, School of Resources, Environment and Materials, Guangxi University, Nanning, China

O. Ola (✉)

Advanced Materials Research Group, Faculty of Engineering, The University of Nottingham, University Park, Nottingham, UK

e-mail: Oluwafunmilola.Ola1@nottingham.ac.uk

1 Introduction

Nanoparticles (NPs) have attracted research interests for over a century and are strongly believed to be the key to future technology due to their large proportion of high-energy nanosized surface atoms compared to bulk materials, which gives rise to outstanding chemical, magnetic, physical, mechanical, catalytic and optical properties. NPs have emerged as an amazing class of materials which is defined within the dimensional range of $\sim 1\text{--}100$ nm. Depending on the overall shape, these materials can be zero-, one-, two- or three-dimensional. For decades, researchers have been paying more and more attention to different metal NPs such as Au, Ag, Pt, Pd, Fe, Co, Mg and Ni, focussing on their synthesis method, characterisations and applications in energy, magnetic imaging, drug delivery, information technology and optoelectronics. Numerous synthesis methods are being established to either enhance the properties or reduce production costs. Furthermore, synthetic techniques and fabrication tools have been continuously studied to permit the production of reproducible nanostructures. It is worth noting that various parameters should also be monitored when NPs are stored due to the changes with time in various environments. Compared to bulk materials, it is sometimes incomplete and inherently difficult to properly analyse the nanomaterials due to the small size and low quantity (i.e. laboratory-scale production). Moreover, the arrangement of particles or atoms in nanostructures brings forth unusual, sometimes exotic forms (e.g. core-shell NPs, fullerenes, nanostructured metals, dendrites, etc.). The NPs characterization is understudied and therefore demands reproducing and validating both theoretical and experimental findings for better scientific understanding, which will benefit the development of new technologies and address important issues, e.g. product lifetimes, etc. Hence, it is important to update new development in the synthesis and characterization of nanomaterials, especially the analysis of their structures, which is believed essential for further progress in nanotechnology. Here in, we explore the nature and causes of a few main NPs synthesis methods and their analytical encounters.

2 Method in Metallic Nanoparticles Synthesis

A wide range of methods have been introduced to produce metal nanoparticles which are categorized into two main types as top-down and bottom-up approaches depending on the starting materials. Hence, bulk materials are usually used as starting materials for the top-down approach while atoms or molecules are typically used for the bottom-up process (Fig. 1). Ball milling, physical vapour deposition (PVD) and lithography are typical top-down methods, while laser pyrolysis, chemical vapour deposition, hydrothermal, sol-gel and electrodeposition are classic methods for the bottom-up approach. However, these all-synthesis techniques are toxic, resulting in environmental contamination; thus, biological methods as an alternative green

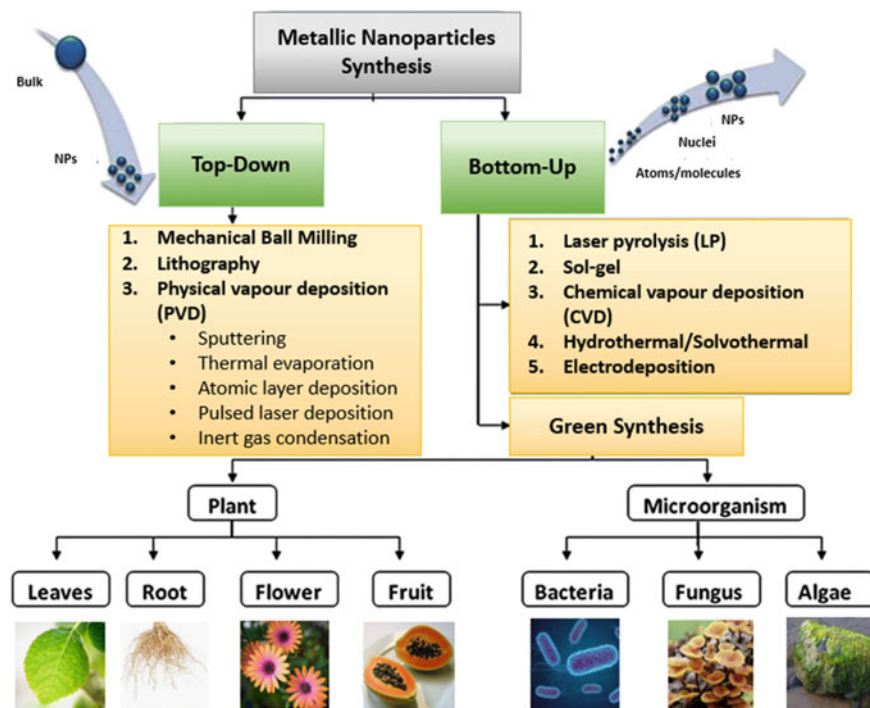


Fig. 1 Summary of metallic nanoparticle synthesis process from both top-down and bottom-up approaches

synthesis were found to be less toxic and environmental friendly. Different preparation methods of metallic NPs create various single or multiple metal (alloy) with different sizes, shapes and structures because of the variation of the parameters during the synthesis process (e.g. stabilizing agent for metallic NPs during the adsorption process, etc.).

2.1 Top-Down Methods

2.1.1 Mechanical Ball Milling

In this method, bulk material which is usually in the micro-dimensions is grounded down to the nanoscale by applying strong mechanical shear forces. Four types of attrition devices are generally used, namely vibration mills, planetary ball mill, tumbler ball milling and attrition mill (as shown in Fig. 2).

Among all top-down methods, ball milling has been widely used for the synthesis of various alloy nanoparticles and composites such as Al, Co, Mg, Ti, Cu and Fe

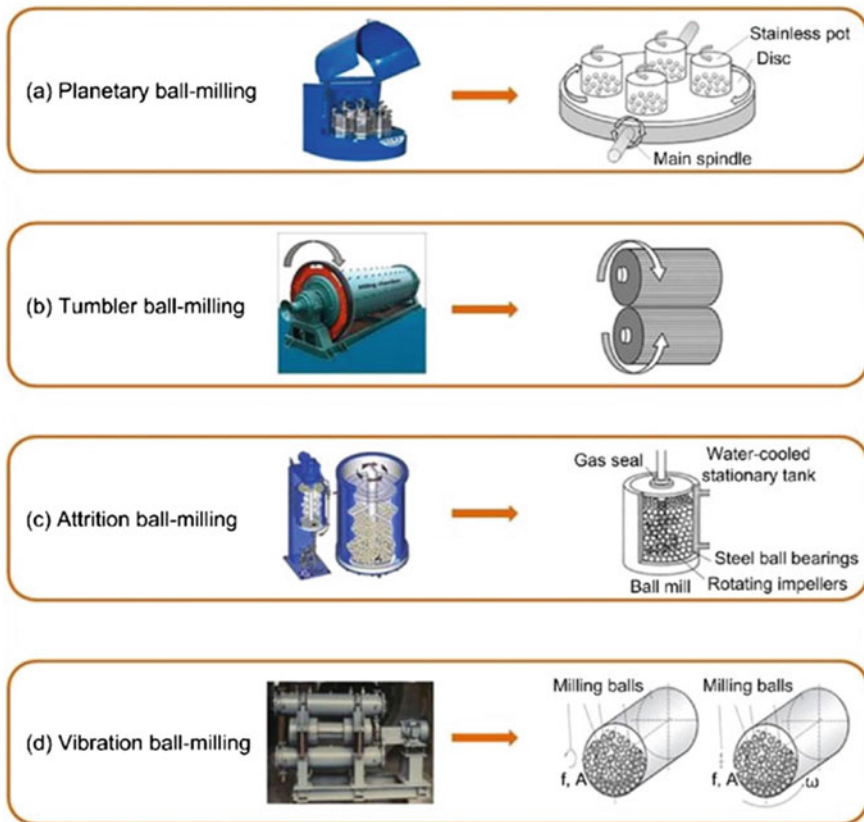


Fig. 2 Different types of ball milling and its working principles: **a** Planetary ball milling, **b** Tumbler ball milling, **c** Attrition ball milling and **d** Vibration ball milling (where f is vibration frequency, A is vibration amplitude and ω is angular velocity) [3]

[4–8]. By using this technique, the nanostructures are fabricated by mechanical attrition, where kinetic energy from grinding balls is used to reduce the size of material [9]. Milling conditions including the size of the milling vial, type of mills (low- or high-energy), milling speed, shape of milling media (balls or rods), milling atmosphere (e.g. inert gas or hydrogen), ball-to-powder weight ratio, milling time, milling environment (dry or wet milling) and milling temperature have a direct effect on properties, stoichiometry, particle size distribution and degree of disorder or amorphization of the final products. A more comprehensive control and monitoring of the milling conditions are suggested to improve the quality of the products.

The raw material's temperature influences the defect concentration and diffusivity inside it, which also influences the phase transformations during milling [10]. Meanwhile, processing time is also a significant factor for this technique. Based on the literature, an increase in time of milling process improves the microhardness of as-prepared materials [11]. Generally, the rate of the internal structure refinement

(e.g. crystallite size, particle size, lamellar spacing, etc.) is roughly logarithmic with processing time and thus the size of the starting materials is relatively unimportant. The lamellar spacing usually becomes small, and the grain size is refined to nanoscale within a few minutes to an hour (Fig. 1); therefore, the milled powders will exhibit increased lattice strain while decreased grain size, hence the resulting milled powders will be in a highly energetic condition [3].

Advantages: Ball milling is well known as a simple, low-production-cost and sustainable technique, and it also possesses the capability to achieve very high yields. The nanoparticle's size ranging from 2 to 20 nm can be achieved through the different speeds of the rotation of the balls. This technique is one of the most reliable, easy-operation and reproducible process because of the speed and energy controls; moreover, it is suitable in both dry and wet conditions for a wide range of materials [4, 7, 12].

Disadvantages: Key serious issue with the milling of fine powders is the possibility of significant contamination from the milling atmosphere or media [4, 7, 9]. Iron contamination can be a problem for steel balls and containers. It has been reported that 10 atomic percentage of the iron contamination in some refractory metallic powders have been found by extended milling times in a high-energy shaker mill. On the other hand, if milling is carried out in open atmosphere, contamination with nitrogen or oxygen can occur. However, optimized milling speed and milling time may effectively help to minimize the contamination issue.

2.1.2 Nanolithography

Nanolithography is one of the most accurate and classic methods for the synthesis of nanoparticle pattern, and it provides high-resolution structures over large areas ($>1 \text{ cm}^2$) with good control of all the dimensions (length, width, height) and other features such as roughness, edge shape and inter-diffusion of the as-prepared materials [13]. This technique is widely used in integrated circuits manufacturing and nanoelectromechanical systems [14]. Lithography can be categorized into 2 main types including masked and maskless lithographies. Masked Lithography utilizes the mask or template to transfer pattern over the large area. The form of mask lithography includes soft lithography, nanoimprint lithography, [15] X-ray lithography and photolithography. On the other hand, maskless lithography technique (including electron beam lithography, Scanning Probe Lithography, etc.) fabricates subjective patterns by a series writing without the use of the mask. In general, the masked lithography has better controllability compared to maskless lithography. Masked lithography is commonly used to prepare nanomaterials that are highly dependent on the specific shape and size of the selected template. The principle of a few different types of lithography is presented in Fig. 3.

Additionally, mask can be classified into 2 types, soft mark and hard mask. Surfactant molecules (e.g. CTAB, TEOS, etc.) are usually used as a soft mask, while polymeric materials (e.g. PDMS PMMA, PS, PFPE and other elastomeric material) are usually used as hard mask [17]. In general, the lithography technique is a three-step

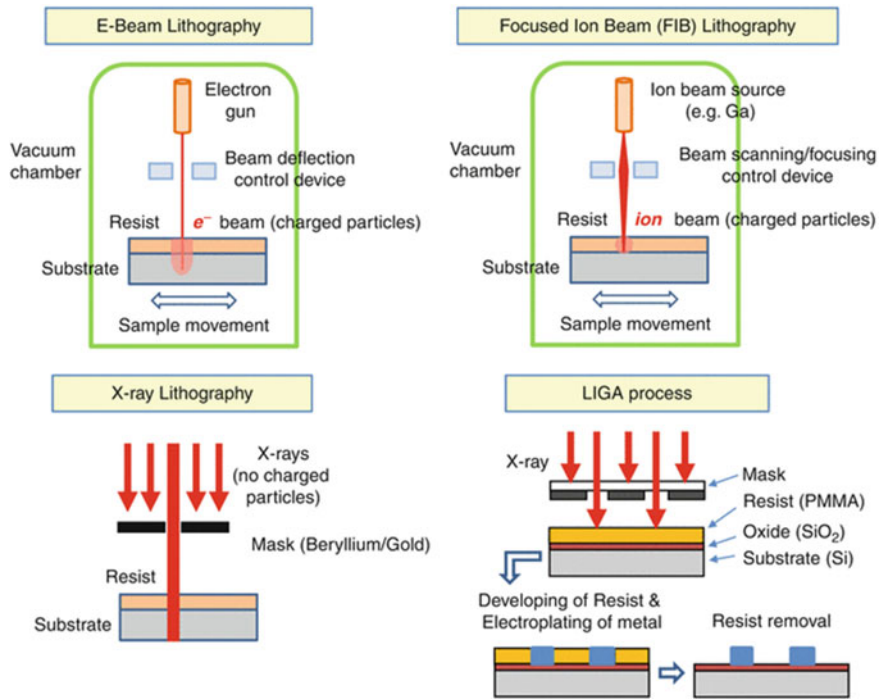


Fig. 3 Different type of mask and maskless lithography technique [16]

process: (1) preparation of a colloidal crystal mask made of nanospheres; (2) deposition of the desired product through the mask; and (3) etching of the mask from the layer.

Sub-10 nm Mo gratings have been successfully prepared by using photolithography [18]. However, the photolithography demands the use of a stepper, which is too expensive to be afforded by a standard research laboratory. Dot arrays can either be achieved using four-beam interference lithography or achromatic Talbot lithography (i.e. high-resolution photolithography) [19, 20]. E-beam lithography can produce features as small as 20 nm of Au NPs, [21] but is very expensive and time-consuming. Hence, it would be reasonable to use photolithography for 5 min while using e-beam lithography for approximately another 5 h to complete a lithographic process. Pros and cons of each lithography techniques are outlined in Table 1.

2.1.3 Physical Vapour Deposition (PVD)

PVD involves either high-temperature evaporation or ions bombardment of solid form materials in vacuum atmosphere; meanwhile, the reactive gas is also introduced into the system to form a compound with metal vapour and then deposited onto the

Table 1 Summary of advantage and disadvantage of lithography technique [22–25]

Type of lithography technique	Advantage	Disadvantage	Applications
Photolithography	<ul style="list-style-type: none"> Well controlled features and high throughput compared to other lithography High-resolution in the range of millimetres to micrometres Low-cost, simple and time-efficient method (i.e. it can create patterns over an entire wafer in a single step) 	<ul style="list-style-type: none"> High up-front cost, e.g. requirement of flat substrate and a mask optical scissors technique for photolithography applications, requirement of clean room facilities, etc Limitation of diffraction at wavelength of 193 nm 	Fabricating integrated circuits such as computer chips and other semiconductor related devices
X-ray Lithography (an advanced version of photolithography)	<ul style="list-style-type: none"> Shorter wavelengths (0.1–10 nm) can be used to solve diffraction limits of photolithography Smaller features can be patterned compared to original photolithography	<ul style="list-style-type: none"> Deformation during the process Vibrations during the process Time-consuming process X-ray masks are very expensive 	Fabricating integrated circuits such as computer chips and other semiconductor related devices
E-beam lithography	<ul style="list-style-type: none"> Capability to provide a small feature compared to those X-ray- and photolithography (be able to custom patterns with sub-10 nm resolution) Fast turn-around time Small wavelength that diffraction no longer defines the lithographic resolution 	<ul style="list-style-type: none"> Scaling error or pattern under-sizing Not ideal process for industrial processing due to high cost of an operation More complex system than photolithography Low production yield per hour upon the different type of electron beam resists 	Cryo-electric, optoelectronic, optical devices, etc
Nanoimprint lithography	<ul style="list-style-type: none"> High cost-effective synthesis technique which is essential for industrial sector Offer a high-resolution structure as fabricated pattern is only limited by the template only Can be used to fabricate nanopatterns at a large scale in a short time (15 wafers/hours per imprint station) High replication accuracy and high preparation efficiency Simply operation process 	<ul style="list-style-type: none"> Require an improvement of the throughput of current approaches to meet the market demand for commercial production The physical nanoimprint mask must be remanufactured by using inflexible mask (hence similar mark that used in e-beam lithography or reactive ion etching) The adhesion between resist and mask is a significant mould problem, it could cause the demand during the procedure of mould release 	Solar cell, Light emitting, plasmonic devices, memory devices, flat panel display, etc

(continued)

Table 1 (continued)

Type of lithography technique	Advantage	Disadvantage	Applications
Scanning probe lithography	<ul style="list-style-type: none"> • Nanopatterns can be created without optical apparatus (i.e. direct writing in nature of the process) • It is capable of highest resolutions less than 10 nm of the pattern, as well as shaping in one-step 3D process • The methods operate under controlled atmospheric conditions, which reduces the tool overhead and costs • The scanning probe capable of detecting surface features down to atomic resolution 	<ul style="list-style-type: none"> • The method is slow inherently slower than, e.g. photolithography or nanoimprint lithography (Super slow 80 nm/s for atomic scale) • The intrinsically low throughput of single probe systems (however, the multiple probes system can be applied to improve this problem) • Limited to specialized device 	Protein patterns, the placement of ferritin nanostructures, electronic devices using quantum effects, etc

substrate as a highly adherent thin film or NPs [26]. PVD can be separated into different types such as *electron beam evaporation deposition (EBD)*, *ion plating (IP)*, *thermal evaporation deposition (TED)*, *pulsed laser deposition (PLD)*, *atomic layer deposition (ALD)*, *cathode arc deposition (CAD)*, *dynamic ion mixing (DIM)*, *electrophoretic deposition and sputtering technique*. The type of evaporation source and deposition substrate is the essential parameter that affect the deposition quality and efficiency. The evolution of size, sharpness and phase of the product also depends on the gas pressure and deposition temperature in the deposition chamber [27]. Typically, this process takes place at the temperature in the range of 100–600 °C and is widely used for fabrication of inorganic thin films (thickness less than 5 μm). PVD coating can be used in a broad range of applications in automotive, aerospace, optical, medical, thin films (e.g. food packaging, Window tint, etc.) and textile industry.

Among all PVD techniques, **PLD** is carried out at low substrate temperatures with a stoichiometry of the target retained in the evaporated films; hence, it is often used for the thin film electrolytes deposition [28]. Two advantages of PLD are the simplicity in process design and the multi-choice of the target forms (e.g. sintered pellet, powder, single crystal, etc.). For the **EBD** technique, both the conductor and insulator can be used as a target. Meanwhile, EBD of organic materials is limited by the decomposition of the molecules. In general, a vacuum environment of 10^{-2} – 10^{-4} Pa, with deposition rates of at least 25 μm/min, is typical condition required for EBD [29]. Moreover, components are commonly preheated in vacuum at temperatures between 800 and 1100 °C, and rotation process is required during the deposition period. EBD is a more efficient choice for evaporating materials with high melting point than other PVD heating and evaporate techniques. However, it is limited for coating the inner surface of complex geometries with the thickness of thin film below 5 nm. The filament degradation in the electron gun could be a cause of non-uniform evaporating rate. The deposition rate of EBD can be obtained up to 100 μm/min depending on the materials and set up conditions [30].

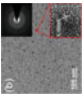
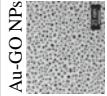
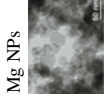
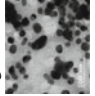
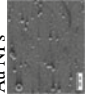
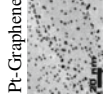
TED technique involves heating a solid material (located in evaporation source, e.g. boat, coil and basket at the bottom of the chamber) to its melting point [31]. The evaporated metal constitutes vapour steam inside a vacuum chamber and then travels across the chamber to the deposition target (located at the top of the chamber), sticking to it as a coating or film. In general, TED of metals with low to moderate deposition rates at 10–100 nm/min provides a simple and reliable manner to produce nanoparticles with a wide range of size; nevertheless, this method is not applicable to substances with high cohesive energies that require high temperature for the evaporation [32]. Material holders are normally made from W, Ta, Mo or ceramic materials that capable of bearing high temperatures. Many materials can be deposited using this method, including Al, Ag, Ni, Cr, Mg, etc. The selection of the PVD technique depends on the material type and possible application. If we are looking for growing thin metallic film, EBD might be the preferred choice compared to the TED. None of PLD technique is better in all aspects. If we are looking for a good step coverage, faster deposition rate, and efficiently, EBD can be preferred, while the sputtering gives you good control on the thickness and density of the films.

Sputtering is good for the deposition of high melting point materials like refractory metals and ceramics, which are tough to be transformed to nanomaterials by evaporation technique. It has been reported that the deposition rates of sputtering technique are much lower than the EBD route (i.e. up to 50 $\mu\text{m/h}$ for a magnetron system or about 10–20 $\mu\text{m/h}$ for a diode system) [33]. Additionally, sputtering offers greater stoichiometric control of the thin film compared to the TED techniques. Thin films from sputtering generally have a higher density than those thin films obtained from the evaporation process while the evaporated films are likely to cause less contamination than those sputtering films because of the lower purity of the sputtering target. **Inert gas condensation (IGC)** is a PVD method with extra function of using the inert gas to reduce the mean value of the free path of the species. IGC technique involves two steps: evaporation of target materials in nanoscale and rapid condensation of the evaporated material. Several different techniques have been employed to evaporate inorganic or metallic materials into a vaporized form, e.g. Joule-heated refractory crucibles, laser/plasma heating or electron beam evaporation devices, etc. Typically, inert gas including He, Ne, Ar, helium, neon, argon, Kr, Xe and Ra with pressures >3 mPa is required during the process [34]. The size and shape of the as-prepared NPs can be managed by different factors including the temperature and pressure of the chamber, evaporation rate and molecular weight of the inert gas that injected into the chamber. A high pressure in the growth region could obtain large particle size due to the consecutive agglomeration and less sintering can be used to synthesize high-purity metallic/bimetallic nanoparticles. It also offers a high surface cleanliness and well-defined grain size with a narrow size distribution of the as-prepared NPs compared to other PVD method. The cost of operation for ultra-high vacuum-based deposition systems of IGC is remarkably high. IGC involves an extremely slow process and suffers from other limitations, e.g. temperature ranges, the source-precursor incompatibility, dissimilar evaporation rates in an alloy, etc.

Advantage: PVD technique can be utilised to deposit a virtually wide range of inorganic materials including metal alloys, ceramics, glass and polymer as well as some of the organic materials. Moreover, it is more environmentally and user friendly compared with other top-down process. The process demands the high vacuum condition to minimize an unwanted reaction within the free space, which helps to shape the film composition easily and causes less contamination on any substrate surface [35]. The purity of the deposited film depends on the vacuum and the quality of the source material. Coating thin film on materials via this technique will offer higher hardness value, more corrosive resistance, good impact strength and excellent abrasion.

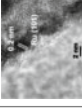
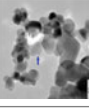
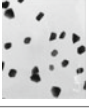

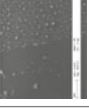
Disadvantage: Difficult to coat undercuts and similar surface feature, high capital cost but low deposition rate. Some PVD processes are typically required to be carried out under high temperature and high vacuum, which cause a high-energy consumption and demands extra attention for operation. Water cooling systems are also needed to dissipate the large heat loads (Table 2).

Table 2 An example of materials that synthesized via different PVD technique

Techniques	Materials	Precursors	Process parameter	Achievement	Application	References
Sputtering deposition	Gd-WO ₃ NPs 	Metallic W target (99.99%) Gd metal slice	RF power 200 W, Ar/O ₂ flow rate ratio 2:3, deposition at room temperature with 0.46 Pa working pressure	139–170 nm of Gd-WO ₃ thin film depending on different amount of Gd dopant	Electrochromic glass	[36]
	Au-GO NPs 	Metallic Au target	Based pressure of 10 ⁻⁸ mTorr with Ar pressure of 2.5 mTorr	Au nanoparticle diameter of 1–6 nm on the GO thin film	–	[37]
	Mg NPs 	Mg target (99.95%)	A base pressure of ~1 × 10 ⁻⁸ mbar, O ₂ pressure of ~10 ⁻⁹ mbar, an inert krypton atmosphere (pressure of ~0.25 mbar)		Mg nanoparticle with diameter of 10–50 nm	Hydrogen storage
Pulsed laser deposition	Ag NPs 	Plates of Ag of 99.99%	Laser pulses at 532 nm with pulse duration of 14 ns, a repetition rate of 20 kHz and an average output power of 6.0 W, electric field of 15 V was applied between the electrodes	Ag nanoparticle with diameter of 20 nm	Development of the synthesis technique	[38]
	Au NPs 	Au target	Laser pulses of energy 0.5 mJ, repetition rate was increased to 3 and 10 Hz, the translation speed at 0.25 mm s ⁻¹ . The ablation depth per shot was ≈100 nm, and the ablated mass was 23 ng. shot-to-shot spacing was 250 μm	Thickness of NPs ranging from 0.4–28 nm upon the changing of the target-substrate separation and the shot-to-shot spacing	Development of the synthesis technique	[39]
Atomic layer Deposition	Pt-Graphene 	Pt (MeCp)Me ₃ , graphene nanoplatelets	About 20 min/cycle. Deposit for 3 cycles at 100 °C. Synthetic air (20 wt % O ₂) was used as the oxygen source, Pt (MeCp)Me ₃ exposure time was 4 min, N ₂ was used as the purging step with step of 5	Ag nanoparticle with diameter below 5 nm	–	[27]

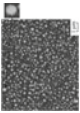
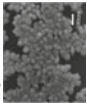
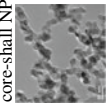
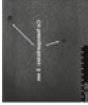
(continued)

Table 2 (continued)

Techniques	Materials	Precursors	Process parameter	Achievement	Application	References
	Ru@CNTs 	Bis(ethylocyclopentadienyl)ruthenium(II)	O ₃ was used as counter reactant. N ₂ was used as carrier with a flow rate of 20 sccm. Reaction chamber temperature of 290 °C. 150 cycles of Ru were deposited to acquire the nanoparticles	3.4 ± 0.4 nm	Catalytic activity in hydrolytic dehydrogenation of methylamine borane (MeAB; CH ₃ NH ₂ BH ₃) and ammonia-borane (AB; NH ₃ BH ₃)	[40]
	Lu@TiO ₂ NPs 	Lu (TMHD) ₃ and Lu (HMDS) ₃	The required dosing time for Lu (TMHD) ₃ and Lu (HMDS) ₃ were 23 and 10 min, respectively. Dosing times were 1.62 (for O ₂) and 2 (for NH ₃) min. During the purge, an additional N ₂ flow of 0.1 l/min (0.30 × 10 ⁻² m/s) was added. Precursor temperature was 210 °C and deposited temperature was 230 °C	No mention clearly about the size of particle	Radio nuclide generator	[41]
Thermal evaporation	Mg NPs  Mg-Zn Nanotriangular 	Mg and Zn metal powders	Base pressure of 10 ⁻⁵ -10 ⁻⁶ mbar, temperatures ranging from 600-800 °C at different holding durations ranging from 1 to 15 min	140-400 nm for Mg nanoparticle, ~45 nm in average. Mg-Zn is hexagonal phase with triangular, platelet like nano structures	Development of the synthesis technique	[1]
	Ni NPs 	Ni powder	Vacuum at 2 × 10 ⁻⁴ mbar Deposition rate: 0.18 nm/Sec at 1.19 Amps to 0.5 nm/Sec at 25 Amps	10 nm of the thin film thickness, size of Ni nanoparticle after heat treatment of the thin film at 700 °C	The annealing effect of thin film	[42]

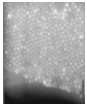
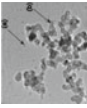
(continued)

Table 2 (continued)

Techniques	Materials	Precursors	Process parameter	Achievement	Application	References
	In NPs 	In powder (99.999% purity)	High-purity Ar atmosphere at a pressure of 6×10^{-5} Pa at different evaporation time of 10, 18 and 30 s	Nanoparticles with dimensions of 10–100 nm and crystallites with dimensions up to 500 nm	Development of the synthesis technique	[31]
	Ag NPs 	Ag wire	Deposited at room temperature in a vacuum chamber under pressure of 2.2×10^{-4} Pa	Ag diameter generally in the range of 40–100 nm	Surface-enhanced Raman scattering (SERS)	[43]
Inert gas condensation	Ni@CoO core-shell NPs 	Ni wire and CoO metal target	Evaporation temperature of 1450 °C by using 150 V ac voltage. W boat and a CoO target was ablated with 20 Hz repetition rate and 4 J/cm ² fluence. Pressure during preparation was 6 Torr. The evaporation rate was 5 g/h and material collection rate at the filter surface was 0.2 g/h	Approximately 4.5 nm diameter core with a shell whose thickness varies in the range of 1.5–2.5 nm	Development of the synthesis technique	[44]
	Cu NPs 	Cu target	A supersaturated vapour of Cu atoms is originated by sputtering a Cu target. The system pressure was 1×10^{-8} Torr. He and Ar are used as inert gases at pressure of 10^{-1} Torr during aggregation. Pressure at the filtering zone is 10^{-4} Torr). Depositing at rates 0.001–0.5 nm/s at condensation zone of 100 mm	Cu clusters in the size range of 1–5 nm	Development of the synthesis technique	[45]

(continued)

Table 2 (continued)

Techniques	Materials	Percussors	Process parameter	Achievement	Application	References
	Fe NPs 	Fe target	Sputtering technique is used as ion source condensation zone length 30–150 mm. magnetron power (25–100 W). Flow of gases, Ar and He with partial pressure $1-2 \times 10^{-1}$ Torr. Deposition time was few minutes up to 30 min	5 nm in average	Development of the synthesis technique	[46]
	Mg NPs 	Manganese granule	The chamber was then sealed and evacuated to around 1.1×10^{-9} mbar. Thermal evaporation at 1533 K. 40 mbar of He is used as carried gas and liquid nitrogen cold trap was used to collect the particles	2–10 nm	Development of the synthesis technique	[47]

2.2 Bottom-Up Methods

2.2.1 Laser Pyrolysis (LP)

LP technique involves the use of a continuous flowing of CO₂, leading to molecular decomposition to form vapours to initiate nucleation, followed by the growth of NPs [48]. On the other hand, some of the other gases such ammonia (NH₃), sulphur hexafluoride (SF₆) and ethylene gas (C₂H₄) are also in use [49]. Next, NPs will be further transported to a filter by an inert gas depending on its amount. The main criterion is that either reactant or precursor should be able to absorb the energy that is supplied through the resonant vibrational mode of infrared CO₂ laser radiations. Inside the system, in most of the time, gaseous precursors are used in LP synthesis; however, solid or liquid precursors can be preferable in many cases, due to safety issues or the cost and availability of the precursor; hence, volatile precursor is not abundantly available for some metals.

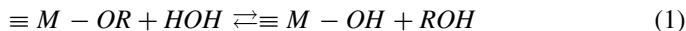
LP provides superfast heating and quenching of particle growth on a small area, hence resulting in rapidly nucleation within few ms. It has been acknowledged that coalescence is higher at the high temperature, resulting in spherical particles, while other shapes are obtained at low temperature. In addition, the final particle size also depends on the aggregation of the initial nuclei. Gas pressure plays a significant role in determining the particle size and their distribution. Moreover, other parameters including laser intensity, the pressure in the reactor cell, the temperature of precursor were also varied in order to obtain different crystallinity and particle size [50]. In general, LP provides more possibilities for NPs with narrow size distribution of 5–200 nm.

Advantage: LP mode provides a very rapid, in-depth heating to a steady-state temperature, offering a high and continuous production of well-dispersed NPs [51]. Moreover, it is the simplest method for producing many nanostructures even at pilot plant dimensions by balancing CO₂ laser exposure and continuous flow of reactor.

Disadvantage: Elevated costs are the main constraints of this method. The requirement of a specific reagent/laser resonance with a specific installation is essential.

2.2.2 Sol–Gel

Sol–gel is a well-known wet-chemical process where a chemical solution acts as a precursor for an integrated system of discrete particles. Among bottom-up synthesis routes, sol–gel is one of the most preferred methods because of its simplicity, easy control of the particle morphology and size, as well as the ability for large volume production of metallic nanomaterial. In general, the method involves two main reactions including hydrolysis of the precursor in the acidic or base mediums (reaction 1) and polycondensation of the hydrolysed products (reactions 2 and 3) [52, 53].



In hydrolysis reaction, an alkoxy group [OR] is replaced with a hydroxyl [OH-]. The part of hydrolysed alkoxide molecules may either react with another OH-species by removing water or react with alkoxy group to produce an alcohol molecule. The hydrolysis reaction rate can be accelerated by using catalyst such as HCl and NH₃. Other parameters such as reagent concentration, ageing and drying process are also important for the structure and properties of final materials network for sol-gel method.

Metal alkoxides (M_x (OR)_y) and chloride compounds are usually used as starting precursors and dissolved in a suitable solvent, which is often ethanol. After completing the hydrolysis/polycondensation reaction process, wet gel product will be dried to obtain the final material (i.e. Aerogel, Xerogel or Cryogel). Ageing process could help to cushion a warping and cracking phenomenon of the gel matrix. Generally, the drying temperature is in the range of 300–500 °C to remove residual organics. Additional calcination or sintering process (temperature up to 800 °C) can also be applied to remove the organic liquid and densify the product in the final step, if required. Normally, the sintering is used for improving the density and reducing of the pore volume and surface area of as-prepared products. On the other hand, calcination often helps in term of mechanically stable of the materials. Xerogel can be obtained from the uncontrolled drying process. It is characterized by disordered porosity in the absence of structure directing agent. Meanwhile, well-controlled drying process to achieve moderate shrinkage of the gel matrix will offer the aerogel type. Hence, drying is the key process to minimize the impact on the porous structure of gel matrix. Figure 4 shows the schematic of sol-gel process from precursor to aerogel.

Parameters such as the ratio of water to alkoxide, the nature of the R-group (e.g. inductive effects) and amount of catalysts strongly affected the reaction of sol-gel process [55]. As an example of silica preparation, the sol-gel chemical reaction normally requires either base or acid catalysts as the neutral reaction is very slow. The structure of the synthesized gel is substantially different depending on the type of additional catalyst as it can offer different in the relative rates of the hydrolysis and condensation reactions. Example of some metallic nanomaterials that synthesized via sol-gel technique is presented in Table 3.

Advantage: This method is simple, highly controllable, economical and efficient to produce high quality and high yield of nanoparticles. Moreover, it can be used for a thick coating to provide protection layer that help to against corrosion of substrate surfaces or used for thin layer coating to ensure a great bond between the top layer and substrate. This method consumes less energy compared to other techniques, especially top-down techniques. There is no need to reach the melting temperature of the precursors for low temperature reaction.

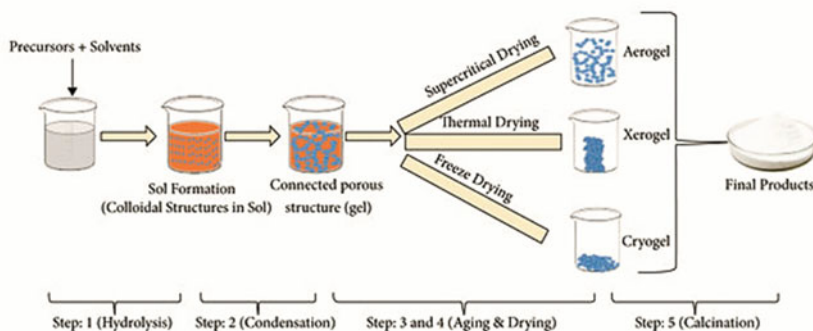


Fig. 4 Schematic of sol–gel process: from precursor to aerogel [54]

Disadvantage: The products often shrinkage and there could be crack formation during drying process, making it difficult to attain a large monolithic piece. The cost of the precursors is high. The process in general involves the use of organic solution that is toxic and harmful to environment. It is hard to avoid residual porosity and OH groups. Finally, the agglomeration issue might occur during the heating process [56].

2.2.3 Chemical Vapour Deposition (CVD)

The key difference between CVD and PVD is that the raw material/precursors for CVD is presented into the reaction chamber in the vapour phase, while the precursors are in solid form for the PVD process. The reaction of CVD process prefers to occur at the substrate rather than in the gas phase. Generally, the temperature ranges from 300 to 1200 °C (higher than PVD process) at the substrate and gas pressures are suggested to be in the range of 0.1 to 1.0 torr. Different factors can affect the deposition process and final produce quality including the precursor delivery method, carrier gas and its chemical properties, the reactor chamber pressure, deposition time and rate, substrate temperature, flow rate of precursor vapour and substrate properties [65]. CVD can be categorized into several types, such as low-pressure, atmospheric-pressure, photo-enhanced, metalorganic and thermal activated CVDs [66].

From Fig. 5, the deposition process can be summarized as three main stages (1) the volatile precursors are introduced to the reactor chamber via carrier gas; (2) the precursor vapours are adsorbed on the substrate surface and then form the intermediate products; and (3) these products are decomposed on the heated substrate, nucleated and grown as the solid layer/grains. The volatile by-products are generated and removed from the chamber by the carrier gas. Growth rate and quality of the

Table 3 Example of some materials that synthesis via sol-gel technique

Metallic nanoparticles	Precursors	Solvent	Catalysts	Polymer skeleton	Ageing temperature and time	Size	Application	References
Au	HAuCl ₄ ·4H ₂ O	De-ionized water	Na ₃ C ₆ H ₅ O ₇ ·2H ₂ O	–	–	20–40 nm	None specify	[57]
Au-siloxane gel	HAuCl ₄ ·4H ₂ O	Methanol and distilled water	Hydrogen tetrachloroaurate(III)	MPTMS and MTMS	Ageing process: 40 °C for 24 h	20–30 nm	None specify	[58]
Au-graphite	HAuCl ₄ ·3H ₂ O, NaAuCl ₄ ·2H ₂ O and pure graphite powder	Distilled water	HCl, Na ₃ C ₆ H ₅ O ₇ ·2H ₂ O, NaBH ₄	MTMOS	Room temperature or 80 °C	<10–20 nm from NaAuCl ₄ 10–20 nm from HAuCl ₄	Amperometric sensing	[59]
Au-Cu-TiO ₂	Au ₂ Cl ₆ , Cu(NO ₃) ₂ , C ₁₂ H ₂₈ O ₄ Ti	Distilled water and ethanol	CH ₃ COOH	–	Ageing: 70 °C for 6 h Calcination: 3 h at 420 °C	3–4 nm of Au NPs	Photocatalyst	[60]
Pt-porous SiO ₂	PtCl ₄	Methanol and acetone	NH ₄ OH	TMOS	Synthesized at room temperature Calcination: 300 °C for 2 h	5–10 nm Pt NPs	Catalyst in heterogeneous reactions	[61]

(continued)

Table 3 (continued)

Metallic nanoparticles	Precursors	Solvent	Catalysts	Polymer skeleton	Ageing temperature and time	Size	Application	References
Ag-SiO ₂	AgNO ₃	Ethanol	HNO ₃	TEOS	Ageing: 25 min at room temperature Drying: 600 °C for 3 h Calcination: 550 °C for 30 min	Average particle size about 10 nm	None specify	[62]
Ag, Cu and Ni	CuSO ₄ , AgNO ₃ , NiCl ₂	De-ionized water and geraniol	NaOH	Starch, PEG and Gelatin	-	70–90 nm for Cu NPs 80–100 nm for Ag NPs 100–120 for Ni NPs	Antibacterial activity	[63]
Au, Ag, Pt, Pd	HAuCl ₄ , AgNO ₃ , H ₂ PTCl ₆ and PdCl ₂	Milli-Q water	Sugar	-	Ageing: 2 h at about 70–75 °C	1, 3, 10 and 20 nm sizes for gold, platinum, silver and palladium, respectively	Synthesis technique	[64]

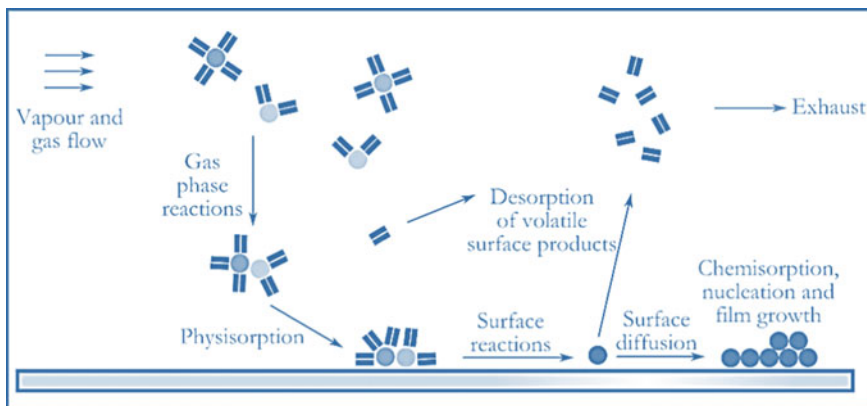


Fig. 5 Reaction in the chemical vapour deposition [67]

thin film depend on the gas pressure inside the reaction chamber and the substrate temperature.

Advantage: CVD offers high uniformity and good reproducibility and adhesion, with acceptable deposition rate [51]. It is not limited to a line-of-sight deposition which is a general characteristic of most of PVD processes. Complex three-dimensional configurations like recesses and holes can be relatively easily coated.

Disadvantage: The synthesis of nanostructures using CVD technique is limited by reason of the involvement of toxic precursors, trace impurities, processing time and prolonged reaction [51]. Possible chemical hazards due to toxic, corrosive and explosive precursor gases. The process typically happened at high temperatures depending on the evaporation temperature of the precursor. Size is limited to reaction chamber capacity.

2.2.4 Hydrothermal/Solvothermal

Hydrothermal/solvothermal synthesis is a solution reaction-based approach, and the reaction temperature could be in a wide range (typically between 100 to 1000 °C). Briefly, the mixed precursor solutions was transferred into lined Teflon and sealed in autoclave made of stainless steel, followed by heating in an oven at a specific temperature and reaction time [68]. Various metal NPs such as Ag, Ni, Cu and Ru [72, 75–78] have been successfully synthesized by using hydrothermal/solvothermal. An image of different NPs is shown in Fig. 6. Crystals with different morphologies (3D-sphere, 2D-rod or 1D-wire structures) are formed by varying the solvent type, concentration of precursor and kinetic control (e.g. reaction time and temperature, etc.).

In general, the reaction medium of hydrothermal synthesis is aqueous solution, while the chemical reaction of solvothermal synthesis happens in various organic

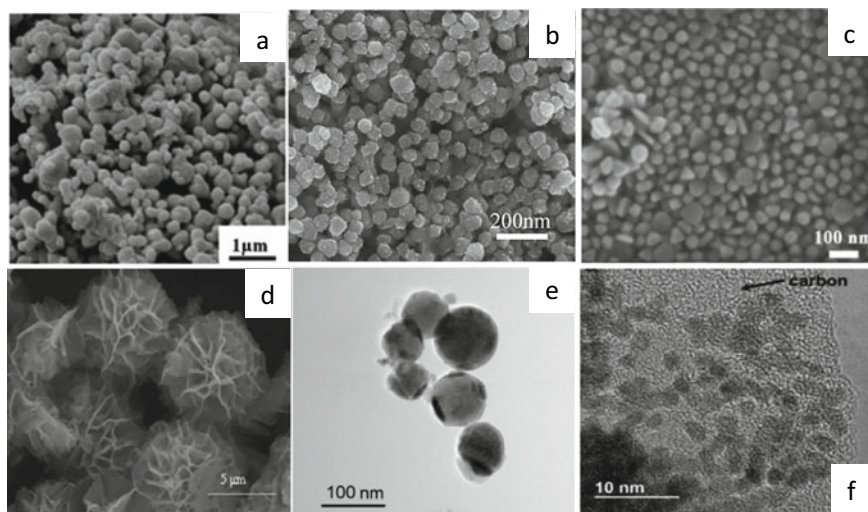


Fig. 6 SEM image of (a) Ag NPs, synthesized at 200 °C for 6 h [71], (b) Cu NPs, synthesized at 100 °C for 10 h, (c) Au NPs, synthesized at 110 °C for 12 h [72], (d) CuS nanostructure, synthesized at 150 °C for 5 h [73], TEM image of (e) Al/Zn NPs, synthesized at 200 °C for 6 h [74] and (f) Ru@C nanocomposites, synthesized at 200 °C for 24 h [75]

mediums. Water has a low boiling point which limits its ability to many reactions that require high-temperature condition. Moreover, water has a high polarity which unable to solubilize many organic and non-polar molecules; hence, capping agents/surfactant (e.g. oleic acid (OA), polyethylenimine (PEI), Ethylenediaminetetraacetic acid (EDTA) and cetyltrimethylammonium bromide (CTAB)) might be needed to stabilize inorganic nanomaterials [69, 70]. Typical precursors for hydrothermal are usually metal-nitrate, -chloride or -acetate compounds.

Advantage: The compositions of nanomaterials can be well simplified and the size, shape distribution and crystallinity in hydrothermal synthesis can be precisely controlled through varying parameters, e.g. temperatures and time of the reaction, the types of precursors, surfactants and solvents. The process can be used to prepare many geometries including bulking powders, single crystals, thin film and nanocrystals.

Disadvantage: Safety issue during the reaction process, high equipment cost (i.e. autoclave) and low products yielded could be the main drawbacks of this technique. Moreover, the reaction process during the reaction cannot be observed. Similar to sol-gel technique, hydrothermal/solvothermal require long time reaction period. This method requires soluble precursor, and large amount of solvent waste can be generated.

2.2.5 Green or Biological Synthesis

Typically, NPs can be achieved by using either microorganisms (such as bacteria, yeast, actinomycetes and fungi) or plant tissues (such as leaf, fruit, root, stem, peel and flower). The synthesis of NPs using a biological system can be categorized into 3 options: (1) using of the solvent medium, (2) using of an eco-friendly and environmentally benign reducing agent and (3) using of a non-toxic material as a capping agent [76]. Several plants and microorganisms have been successfully used for efficient extracellular synthesis of different metal NPs such as Co, Cu, Ag, Au, Pd and Pt as presented in Table 4. Factors including pH, reaction time, reactant concentration and reaction temperature can be adjusted to control the size, shape, yield and stability of as-prepared NPs from the biological synthesis [77].

NPs produced by bacteria offer a very good stability, well dispersion and activities against various pathogens. Fungi are able to produce metal nano- and meso-structures by reducing enzyme intra- or extra-cellularly with the biomimetic mineralization procedure [77]. Using different species of fungi as nano-biofactories for synthesis process is considered more straight forward and easy for stable production of NPs as compared to bacteria. Fungi offers several advantages over bacteria including (1) higher bioaccumulation of metabolites, (2) higher biomass and easy mode of culture, (3) higher wall binding capacity of metals and (4) higher tolerance and uptake capability of metals.⁷⁸ Yeasts according to invention are classified into the kingdom Fungi and class Saccharomyces. One main advantage of using yeast cells as NP-carriers is simple encapsulation mechanism which implies that the synthesis process does not require stabilizers compared to other NP-carrier system.


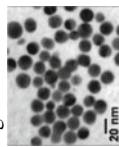
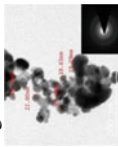
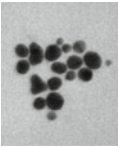
Advantage: Green synthesis eliminates the use of chemicals and offers non-toxic products and by-products. Moreover, it can also generate a large amount of highly stable NPs with a better-size distribution than those chemical and physical methods due to non-nutrient bioactive compounds (as stabilizing agents) that are used in the reaction act [79].

Disadvantage: The large-scale production protocols of this technique require further modification to make them cost-effective and comparable to other methods. Instability and aggregation of NPs, control of morphology, crystallization and size of NPs via this technique are under the development stage. Moreover, the separation and purification process of NPs is another key issue that needs further exploration.

3 Methods Used in Metal Nanoparticles Characterization

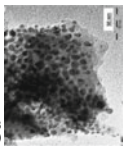
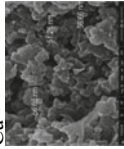
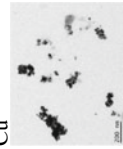
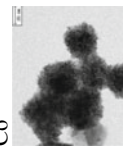
Understanding the characteristics of NPs benefits in validating the fabrication technique, succeeding the morphology evolution, improving the method protocols and realizing the potential applications of the NPs. Characterization techniques can be classified based on the concept of the techniques used, the provided information or the types of materials that required for the technique. The main features of the techniques and their key benefit, advantages and limitations are explained and pointed

Table 4 Example of NPs synthesis from various biological sources [80–84]

Plants	Type of metallic nanoparticles	Bio-reducing agent	Size of nanoparticles	Application	References
	 	Aloe vera (Leaf)	10–30 nm	Optical coatings and cancer hyperthermia	[85]
		Tectona grandis (seed)	<30 nm	Antimicrobial activity	[86]
		Polyscias scutellaria (Leaf)	~5–20 nm	Catalytic Activity to Reduce Methylene Blue	[87]

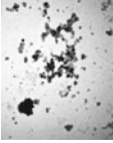
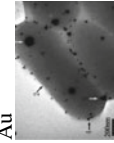
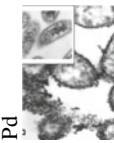
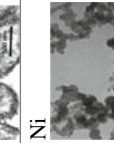
(continued)

Table 4 (continued)

Type of metallic nanoparticles	Bio-reducing agent	Size of nanoparticles	Application	References
Cu 	<i>Celastrus paniculatus</i> (leaf)	~2–10 nm	The antifungal activity	[88]
Cu 	<i>Fortunella margarita</i> (Leaf)	~51–56 nm	Development of synthesis process	[89]
Cu 	<i>Cissus vitifera</i>	10–20 nm	The antioxidant and antibacterial activity against urinary tract infections pathogens	[90]
Co 	<i>Asparagus racemosus</i> (root)	20 nm	Antibacterial activity	[91]

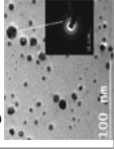
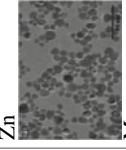
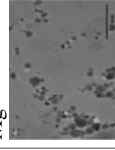
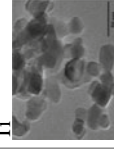
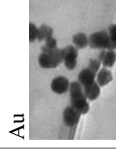
(continued)

Table 4 (continued)

Bacteria	Type of metallic nanoparticles	Bio-reducing agent	Size of nanoparticles	Application	References
Ag		Bacillus cereus	20–40 nm	Antibacterial activities	[92]
Au		Escherichia coli DH5 α	about 20 nm	electrochemistry of haemoglobin	[93]
Pd		Sulfidogenic	~10 nm	Development of synthesis process	[94]
Ni		Escherichia coli and Staphylococcus aureus	70–90 nm in average	Magnetic mirror with antibacterial activities	[95]

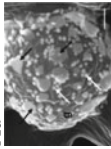
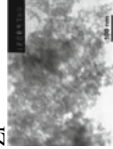
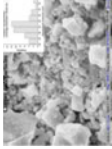
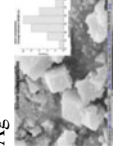
(continued)

Table 4 (continued)

Fungi	Type of metallic nanoparticles	Bio-reducing agent	Size of nanoparticles	Application	References
Ag		Rhizopus stolonifer	NPs size ~2.86 nm was produced at 40 °C NPs size ~25 and ~48 nm was produced at 20 and 60 °C, respectively	Development of synthesis process	[82]
Zn		Soil-borne	Zn: 15–88 nm Mg: 10–96 nm Ti: 13–17 nm The size varies depended on various precursor compound	Development of synthesis process	[96]
Mg					
Ti					
Au		Bacillus niabensis 45	~20 nm	Antibiofilm activity	[97]

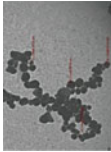
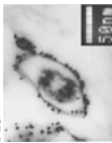
(continued)

Table 4 (continued)

	Type of metallic nanoparticles	Bio-reducing agent	Size of nanoparticles	Application	References
Yeast	Au 	Yarrowia lipolytica NCIM 3589	Varying	Development of synthesis process	[98]
	Zr 	-	2.7 nm	Fuel cell technologies	[99]
Algae	Cu  Ag 	Botryococcus braunii	Ag and Cu NPs were found to be in the range of 40–100 nm and 10–70 nm, respectively	Antimicrobial Activity	[100]

(continued)

Table 4 (continued)

Type of metallic nanoparticles	Bio-reducing agent	Size of nanoparticles	Application	References
Ag 	Gelidium corneum	20–40 nm	Antibiofilm activity	[101]
Au 	Tetraselmis cochiniensis	~15 nm	Catalysis, electronics, coatings	[102]

out in this session. Table 5 summarizes the techniques that are suitable for different focus characterized parameter of NPs.

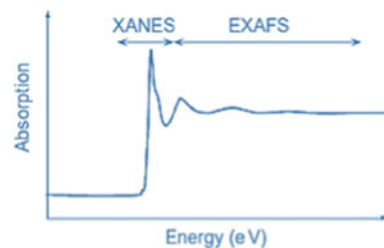
Table 5 Characterization techniques for NPs parameters [103, 104]

Entity characterized	Suitable characterization techniques
Size (structural properties)	TEM, XRD, DLS, NTA, SAXS, HRTEM, SEM, AFM, EXAFS, FMR, DCS, ICP-MS, UV-Vis, MALDI, NMR, TRPS, EPLS, magnetic susceptibility
Shape	TEM, HRTEM, AFM, EPLS, FMR, 3D-tomography
Elemental-chemical composition	XRD, XPS, ICP-MS, ICP-OES, SEM-EDX, NMR, MFM, LEIS
Crystal structure	XRD, EXAFS, HRTEM, electron diffraction, STEM
Size distribution	DCS, DLS, SAXS, NTA, ICP-MS, FMR, superparamagnetic relaxometry, DTA, TRPS, SEM
Chemical state-oxidation state	XAS, EELS, XPS, Mössbauer
Growth kinetics	SAXS, NMR, TEM, cryo-TEM, liquid TEM
Ligand binding/composition/density/arrangement/mass, surface composition	XPS, FTIR, NMR, SIMS, FMR, TGA, SANS
Surface area, specific surface area	BET, liquid NMR
Surface charge	Zeta potential, EPM
Concentration	ICP-MS, UV-Vis, RMM-MEMS, PTA, DCS, TRPS
Agglomeration state	Zeta potential, DLS, DCS, UV-Vis, SEM, Cryo-TEM, TEM
Density	DCS, RMM-MEMS
Single particle properties	Sp-ICP-MS, MFM, HRTEM, liquid TEM
3D visualization	3D-tomography, AFM, SEM
Dispersion of NP in matrices/supports	SEM, AFM, TEM
Structural defects	HRTEM, EBSD
Detection of NPs	TEM, SEM, STEM, EBSD, magnetic susceptibility
Optical properties	UV-Vis-NIR, PL, EELS-STEM
Magnetic properties	SQUID, VSM, Mössbauer, MFM, FMR, XMCD, magnetic susceptibility

3.1 X-Ray-Based Techniques

- *X-ray diffraction (XRD)* is a basic technique for NP characterization which provides the information of the crystalline structure, phase, lattice and grain size of NPs [105]. XRD is commonly used for powder or thin film samples. The composition of the NPs can be identified by comparing the position of the 2-theta peaks with the standard patterns (i.e. ICDD, or known as JCPDS) database [103]. In general, the intensity of X-ray source is about [108] times lower than that of the electron diffraction.
- *X-ray photoelectron spectroscopy (XPS)* is a highly surface-sensitive analysis method, giving information of electronic structure of NPs and charge transfer between constituent elements in alloy and/or heterostructure NP's surface [106]. Moreover, it is also possible to extract the element and phase composition of the NPs from surface analysis data. Binding energy presented an information of the element, whereas the peak intensity reflects the relative concentration of the elements [107]. Background subtraction and peak fitting methods are required for an analysis of the complex element that has several oxidation states.
- *X-ray absorption spectroscopy (XAS) includes both extended X-ray absorption fine structure (EXAFS) and X-ray absorption near edge structure (XANES, also known as NEXAFS).* XAS is involved in the measurement of X-ray absorption coefficient of NPs as function of energy (Fig. 7.) [108]. In principle, each element has a set of characteristic absorption edges (i.e. K, L, M, etc., absorption edges) according to the different binding energies of its electrons, offering XAS element selectivity. In other words, this technique offers result of the chemical composition, unoccupied electronic states and bonding information of the NPs [109]. A highly sensitive EXAFS techniques can be used to gain the information about the interatomic distances, near neighbour coordination numbers and lattice dynamics. On the other hand, XANE gives information about the oxidation states, vacant orbitals, electronic configuration and site symmetry of the absorbing atom.
- *Energy-dispersive X-ray spectroscopy (EDS) and X-ray scattering (SAXS)* are used for the elemental analysis or chemical characterization of NPs. Each chemical element has characteristic X-ray energy that emitted from the specimen. EDS is typically combined with SEM and TEM, allowing a clear identification of the composition of elements heavier than oxygen.

Fig. 7 XAS spectrum shows the edge XANES (within ca. 50 eV) and the edge EXAFS (>1000 eV above) of the structured absorption [110]



3.2 *Fourier Transform Infrared Spectroscopy (FTIR)*

FTIR is used for studying the vibration of the functional groups associated with NPs. FTIR records the absorption of electromagnetic radiation with wavelengths within the mid-infrared region ($400\text{--}4000\text{ cm}^{-1}$) [111]. If a molecule of NPs can absorb infrared region radiation, the dipole moment somehow changed, and the molecule becomes IR active. A spectrum not only offer the information of band position related to nature and strength of bonds, but also determine the specific functional groups, which can help to obtain the information of molecular structures and interactions of NPs. In general, powder samples will be grounded with KBr (about 5% of the weight of the samples) and pressed to form the hard pellet [112].

3.3 *Transmission Electron Microscopy (TEM)*

The interaction between an electron beam with uniform current density and a thin sample can be observed by using TEM as the beam is transmitted through that thin film samples to form an image. In general, the energies of the electron beam are within a range of 60–150 keV. TEM is the most common technique to analyse morphologies of NPs as it can provide not only direct images of the sample but also the most accurate estimation of the NPs homogeneity due to its powerful magnification with the potential of over 1 million times compared to other SEM techniques.

High-resolution TEM (HRTEM) is an imaging mode of TEM that uses phase-contrast imaging, using the combination of transmitted and scattered electrons to produce the image of the internal structure of NPs (i.e. the arrays of atomic level in crystalline structures of NPs). It is worth mentioning that the internal structure characterization of amorphous-based structure is not always practicable by this HRTEM technique due to the random orientation of their crystals relative to the electron beam; hence, the atom directions are not well aligned, obtaining a complex image that cannot be directly used for structural analysis. Selected area electron diffraction (SAED) or an electron backscatter diffraction (EBSD) in TEM is used for the study of the crystal structure of NPs, obtaining the reverse space of the lattice planes as it can be used to determine the d-spacing value of the crystal planes of the NPs.

3.4 *Scanning Electron Microscopy (SEM)*

SEM is another common technique for imaging of nanomaterial surface with a resolution down to about 1 nm [113]. SEM uses electrons where the incident beam of electrons transversely scans the sample, offering data on the composition of atoms along with the physical feature of NPs [114]. The focussed beam of electrons can be able to create a magnified image with much improved magnification of 10 to

1,000,000 times. SEM usually uses three analysis modes including (1) secondary electron (SE) mode, (2) backscattered electron (BSE) mode and (3) X-ray energy dispersive spectroscopy [115]. A classic SE mode can obtain image with up to 1 nm resolution. However, SEM is limited when used to characterize non-conductive materials and coloured images (i.e. SEM only provide black and white image), or when used to acquire the height of the specimen. Coating the samples (sputter coating) with an additional conductive material layer of $\sim 3\text{--}10$ nm (such as Pt, Ag, Pd and Au) is required, especially for non-conductive sample to remove charging effects and get better quality images of the sample. However, the thin layer of conductive materials (from sputtering) may affect the atomic percentage and elemental composition analysis of the NPs.

3.5 Atomic Force Microscopy (AFM)

AFM is capable of creating 3D images of surfaces with high magnification. The measurement of this technique is based on the interacting forces between the sample surface and a probe. AFM can scan under three different modes (i.e. contact, non-contact and tapping mode) depending on the degree of proximity between the probe and the sample. Parameters including tip curvature radius and elasticity and surface energy of NPs influence the final topological values. AFM does not require any surface modification or coating prior to imaging; hence, it does not require a coating of conductive layer on the surface of non-conductive materials as SEM technique. Moreover, the topological analysis of small NPs (≤ 6 nm) can be obtained by AFM without requirements of the special treatment. Low density materials, which present poor contrast in electron microscopy, can also be characterized. For comparison, Fig. 8 shows the image of copper/1,4-benzenedicarboxylate (N-Cu(BDC) composite that taken by AFM, TEM and SEM.

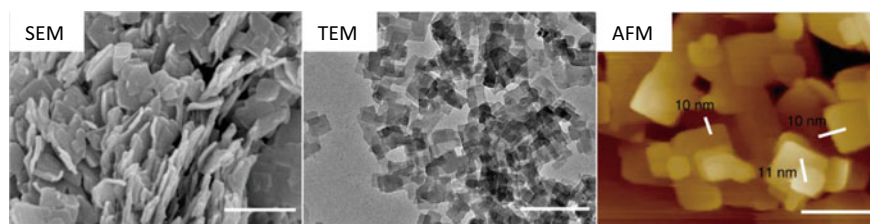


Fig. 8 An example of SEM, TEM and AFM of N-Cu(BDC) composite [104]

3.6 *Dynamic Light Scattering (DLS)*

DLS provides the measurement of the size of the NPs from the scattered light in a solution; hence, it is difficult to imaging dried samples and very sensitive to agglomeration and dynamic aggregation [116]. As the DLS directly characterizes particles in dispersion, dispersion conditions including the effect of salt or pH on colloidal stability can be monitored [117]. This method can be used to analyse in a great diameter ranging from nano- to micro-scale. However, it cannot directly observe the size of NPs from the DLS result as the mechanism of method is based on diffusion coefficient value, and the spherical shape of the particles is therefore assumed. Hence, the dimensions of a particle can only be defined by using an assumption of shape by Stokes–Einstein equation [115].

3.7 *Zeta Potential Measurement*

Zeta potential or an electrokinetic potential is a measurement of the “effective” electric charge at the slip plane between the bulk of base solution and the bound layer of diluent molecules that surrounds the NPs. Hence, this technique measures the charge stability of colloidal NPs, which is a key parameter that governs the electrokinetic behaviour of NPs in the solution [118]. In general, NPs with a zeta potential value between -10 and $+10$ mV are considered as neutral, while NPs with zeta potentials value of less than -30 mV or greater than $+30$ mV are considered strongly anionic or strongly cationic [119]. Zeta potential is dependent on pH and the conductivity of the dispersing medium; thus, it is important to accurately measure and report it. For example, if acid is added in nanofluid, pH will decrease, leading to the increase of positive charges on the particle surface. The minimum concentration required for analysis depends on the relative refractive index and particle size. Additionally, this technique some time can be used to predict the long-term stability of colloidal NPs. For example, NPs with zeta potentials larger than ± 60 mV have great stability, whereas when zeta values of NPs are between -10 mV and $+10$ mV, a rapid agglomeration can be observed unless they are sterically protected [120].

3.8 *Secondary Ion Mass Spectrometry (SIMS)*

SIMS is one of the key techniques for surface chemical and imaging analysis in the field of material sciences. This technique is recognized as isotopic surface analysis and the most sensitive elemental analysis technique. In the chamber, the sample is bombarded with an ion beam in vacuum atmosphere; thus, the secondary ions are sputtered from the sample and conveyed into a mass spectrometer for analysis [121]. The SIMS technique provides a unique combination of extremely high sensitivity

which limits down to the ppm level for all elements from Hydrogen to Uranium and above. Moreover, it also offers high lateral resolution imaging (≥ 40 nm), and a very low background that allows more than 5 decades of dynamic range.

3.9 UV–VIS Spectrophotometry

It is widely known that metallic NPs possess multi-colours and, therefore, best matched for photo-related applications. Figure 9 shows characteristic colours and properties of Au NPs with the variation of sizes and shapes, which can be utilized in imaging-related applications [105]. Ultraviolet–visible (UV–Vis) and photoluminescence (PL) are the well-known techniques for the optical study of NPs materials [105]. Both techniques offer extra information about the absorption or emission capacity of the NPs and their effect on the overall excitation time of photo-excitations. Additionally, UV–Vis can quantitatively monitor the formation and provide information about the size of NPs through different responses to the electromagnetic waves, ranging from 200–700 nm [122] (Table 6).

Fig. 9 Colour dependence of Au NPs on size and shape [105]

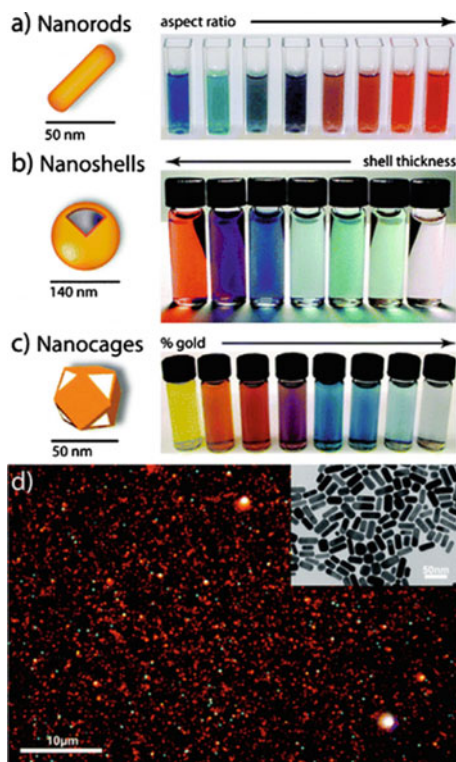


Table 6 Summary of advantage and limitation of the techniques that are used for NPs characterization in this paper [123, 124]

Role	Advantage	Limitations	Sensitivity	References
SEM	<p>Topographical, morphological and compositional information (i.e. combined with EDS system)</p>	<ul style="list-style-type: none"> Imaging at all directions through x-y-z (3D) rotation of sample is possible Easy to be integrated with digital camera systems for data storage and analysis Allows a large amount of the sample to be focussed at one time compared to TEM 	<ul style="list-style-type: none"> Limited to solid sample and must be operated under vacuum conditions SEM must be in an area free of any possible electric, magnetic or vibration interference Low resolution compared to TEM, usually up to sub-micron or a few hundreds of nanometres Required surface stain-coating with metals for electron conducting 	Down to 1 nm [125]
TEM	<p>Morphology (particle size and shape); crystallographic information (detection of atomic scale defects); compositional information (STEM); the phases that present (i.e. lattice spacing measurement)</p>	<ul style="list-style-type: none"> TEM offers the highest resolution compared to other morphological analysis technique Direct imaging of crystalline lattice of sample No metallic stain-coating is required to assign the defects inside the sample 	<ul style="list-style-type: none"> Required ultra-thin sample (thickness below 200 nm) Sample might be damaged by electron beam during process Expensive equipment installation, i.e. vacuum system, is required for atomic scale resolution The difficulty in quantifying multi-particles or misleading images due to orientation effects Limited to solid sample 	0.1 nm [124, 126]
AFM	<p>Shape, texture and roughness of individual particles and their distribution for an assembly of particles</p>	<ul style="list-style-type: none"> Can be operated in vacuum/air/liquid, unlike TEM and SEM that required to operate in the vacuum chamber High lateral magnification is not required for AFM, while lateral magnification is an important factor in TEM and SEM method Incapable of characterizing the height or z-axis of NPs 	<ul style="list-style-type: none"> AFM has slower scanned times than any kind of electron microscopy Tip shape can become convoluted with measurements Unable to obtain qualitative or quantitative information of the sample composition (i.e. cannot provide direct chemical information) 	1 nm (XY), 0.1 nm (Z) [104]

(continued)

Table 6 (continued)

Role	Advantage	Limitations	Sensitivity	References
DLS Measuring the hydrodynamic size and size distribution of molecules and particles	<ul style="list-style-type: none"> Fast, easy handling, non-invasive and used under a wide variety of solvent conditions Requiring a low volume of the sample and can be easily implemented as an in-line quality control method less labour intensive and an extensive experience is not required for routine measurement Fast, no sample preparation and sample preservation from downstream analysis 	<ul style="list-style-type: none"> Measurement of size is inaccurate with heterogeneous samples Requires adapted sample dilutions Offering highly sensitive analysis of NPs, which might be possible to detect unwanted size fractions from unclean lab-ware, dust and aggregated sample Cannot separate particles and agglomerations 	3 nm	[124, 127, 128]
XRD Size and crystal structure (long range order) measurement of NPs- lattice parameter, internal stress/strain (elastic), coherently scattering domain size (crystallite size)	<ul style="list-style-type: none"> The most convenient, inexpensive compared to those other technique Best method for phase analysis 	<ul style="list-style-type: none"> High intensity x-ray beam required (i.e. synchrotron x-ray source) X-ray do not interact very strongly with lighter element Complex composition of NPs and plasmon cannot be found The shrinkage of the lattice space by XRD may be complicated, as instrumental parameters, reflection broadening due to a very small NP size and matrix effects can lead to unclear XRD results 	Down to 1 nm	[129]
XPS Qualitative and quantitative elemental composition of the surface layers, chemical state identification and density of electronic states	<ul style="list-style-type: none"> High accuracy in identifying samples Suitable for both conductive and non-conductive materials Suitable for both inorganic and non-organic 	<ul style="list-style-type: none"> Very expensive technique Slow process (30 min–8 h per sample) H and He cannot be identified Sample must be compatible with high vacuum environment 10% relative error in repeated analyses 	3–92 nm	[106–107, 130]

(continued)

Table 6 (continued)

Role	Advantage	Limitations	Sensitivity	References
XAS Absorption energy, element valence state, charge transfer and type of bonding information	<ul style="list-style-type: none"> Can focus on one element without interference from other elements present in the sample Ability to analyse almost any type of samples including amorphous (non-crystalline) materials Determination of the element oxidation state, data which often difficult to obtain by other spectroscopic methods 	<ul style="list-style-type: none"> Cannot be used to study low atomic number element Difficult to deconvolute the bulk data when the sample is composed of a mixture of structures of the absorber element 	5–6 Å	[108, 131, 132]
EDS Evaluation of chemical composition of the particles	<ul style="list-style-type: none"> Composition of NPs can be analysed via various modes, i.e. Elemental mapping, point analysis, line analysis and area analysis 	<ul style="list-style-type: none"> EDS is generally not a particularly sensitive technique. If the concentration of an element in the sample is too low, EDS might not be enough to adequately measure its proportion EDS generally does not work for elements with a low atomic number, e.g. H and He 	<2 nm	[104]
FTIR Nature of bonds and functional groups measurement	<ul style="list-style-type: none"> FTIR provides the fastest scan rate among all of the dispersive instruments The FTIR instrument does not limit the amount of light reaching the detector using a slit, unlike other structure instruments (hence, more energy reaches the sample, thus less reflective losses occur) 	<ul style="list-style-type: none"> The changes in their spectra are not significant enough to provide clear evidence for nanocomplex formation (because of low sensitivity or peak overlapping) Structure and size of NPs cannot be measured 	20 Å–1 μm	[112, 133]

(continued)

Table 6 (continued)

	Role	Advantage	Limitations	Sensitivity	References
SIMS	Presence of surface coatings or contaminants on collections of nanoparticles, functional groups on surface of NPs	<ul style="list-style-type: none"> • Can provide molecular information about film and particles surfaces • Determine the presence of trace elements 	<ul style="list-style-type: none"> • Most instruments cannot characterize individual particles, therefore requires a collection of particles • Needs appropriate sample preparation and handling to minimize information loss • Sputter rates accelerated for nanoparticles • Nanoparticles can melt or transform, sputtering can destroy the size, shape and composition of the particles • Requires vacuum 	50 nm (x, y), 1 nm (z)	[134]
UV-VIS	Optical properties, concentration and shape of NPs can be measured	<ul style="list-style-type: none"> • Rapid analysis, reliable, easy to handle, high precision and accuracy • Available on various sample forms, e.g. colloidal solutions, suspensions, thin films and powders 	<ul style="list-style-type: none"> • Solid particles in a heterogeneous sample scatter light more than they absorb it; hence, the data are doubtful. Restriction to turbid samples 	UV-visible regions 200–800 nm	[124, 135]

4 Basic Properties of Metallic Nanomaterials

4.1 Surface Plasmon Resonance Properties

Among metals, noble metals including Au, Ag, Cu, Pd and Pt gain a great attention due to their exclusive optical properties on account of their surface plasmon resonance (SPR), which can be applied in a broad range of applications such as photocatalysis, biomedicine, surface-enhanced Raman spectroscopy (SERS), plasmonic devices, sensors and photothermal therapy [136, 137]. Among these plasmonic NPs, silver and gold are most used as plasmonic metals because of their chemical stability and visual colour change to the naked eye. On the other hand, Pt or Pd exhibit only broad absorption which continuously extend throughout the near UV and visible range.

Noble metal NPs exhibit a strong UV–vis absorption band, which is not possessed by bulk metals. This absorption band is provided by the collective oscillations of electrons in the conduction band that excited by light with appropriate frequency from both visible and near-infrared ranges, which is known as localized SPR [138]. The position of the plasmon band (extinction spectrum) is best measured on a conventional UV–visible spectrophotometer, observing a band with high extinction coefficients (up to 10^{11} /M.cm) [139]. The optical features of the localized SPR (e.g. peak absorption, peak extinction wavelength, scattering, linewidth) depend on the size, shape, composition of the metal NP, surface-adsorbed species, surface charge, interparticle interactions and the refractive index of the surrounding medium [140]. An example of optical value change of Au and Ag NPs that depend on their shape is present in Fig. 10.

4.2 Magnetic Properties

Magnetic properties of metal NPs are of great interest for a wide range of disciplines, such as magnetic fluids, catalysis, biomedicine, magnetic energy storage, information storage and spintronics [141]. Fine particle magnetism comes from size effects, which are based on the magnetic domain structure of ferromagnetic materials. When the size of single-domain particles is reduced below a critical diameter (<15 nm for the common materials), the coercivity is zero and such particles become superparamagnetic, which is caused by thermal effects. Each potential application of the magnetic nanoparticles requires different properties. Materials that hold ferromagnetism (e.g. Fe, Ni and Co) have aligned atomic magnetic moments of equal magnitude; thus, their crystalline structures allow for direct coupling interactions between the moments, which helps to enhance the flux density of material [142]. Many studies have confirmed low toxicity of AuNPs compared to other metal-based NPs [143], Au (3.9 ± 0.2 nm) has been used to decorate peI-Fe₃O₄ (Au@PEI-Fe₃O₄) NPs and their DC magnetization. The estimated effective magnetic anisotropy constant (K_{eff} ,

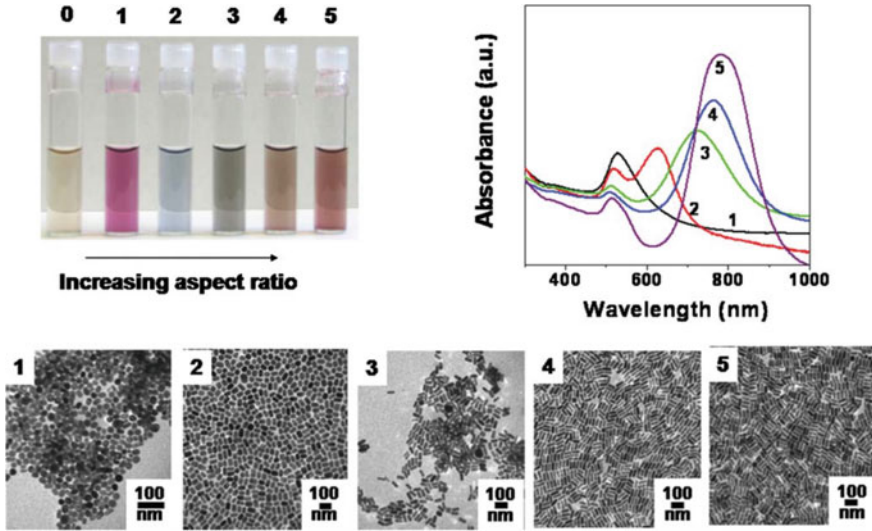


Fig. 10 A different shape of Au and Ag NPs can directly influence the change in their optical performance. Vial 0 presented the aqueous solution of 4 nm Au nanospheres and Vial 1–5 presented the higher aspect ratio gold nanorods [140]

at 5 K) was $2.0 \times 10^4 \text{ j/m}^3$, nearly 50% larger than K_{eff} of bulk magnetite ($1.1\text{--}1.3 \times 10^4 \text{ j/m}^3$) (Fig. 11) [144].

4.3 Mechanical Properties

The mechanical properties of NPs have gained a lot of attention over the last few years especially the tribological properties for lubricants and as reinforcements for composite coating technologies [145, 146]. In general, the mechanical properties of material involve elastic–plastic deformation, hardness, bulk modulus, Young’s modulus, scratch resistance, time-dependent creep and relaxation properties, residual stresses, fracture toughness, fatigue and yield strength. Au NPs thin films have been well studied for their high hardness, creep and strain rate effects [147]. However, the obtained results are still insufficient and some are controversial [148, 149]. There is still no conclusion whether the elastic modulus of NPs is affected by the particle size and the indentation depth. Additionally, their frictional and mechanical behaviours have not been fully understood. A study has recently reported the ultra-high compressive strength of the Ni NPs of 34 GPa ($D \approx 210 \text{ nm}$), as shown in Fig. 12 [150].

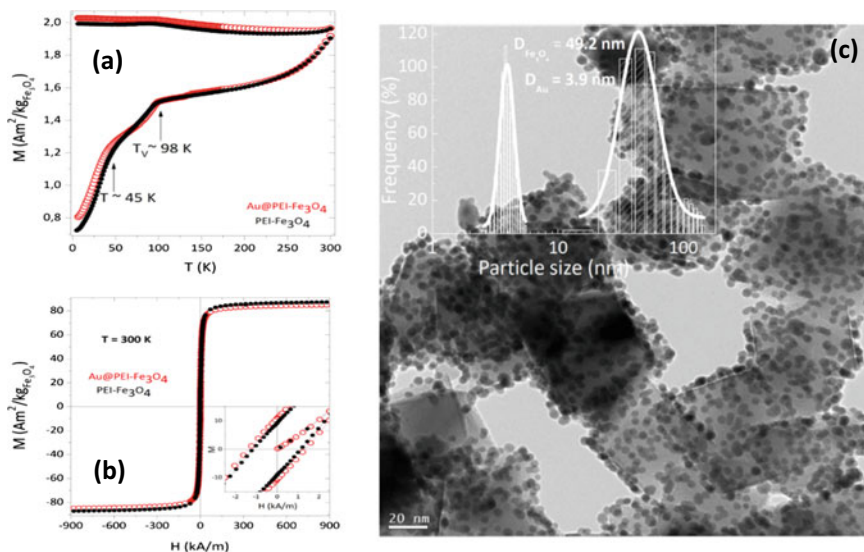


Fig. 11 **a** DC magnetization curves gained in zero-field-cooled (ZFC, lower branch) and field-cooled (HFC = 2.39 kA/m, upper branch) modes for PEI- Fe_3O_4 (filled black circles) and Au@PEI- Fe_3O_4 (open red circles) NPs. **b** M vs. H curves at $T = 300$ K. Inset: magnification of the low-field region of the hysteresis loops. **c** TEM of Au@PEI- Fe_3O_4 NPs, inset: the histogram of particle fitted with a lognormal distribution (solid line) [145]

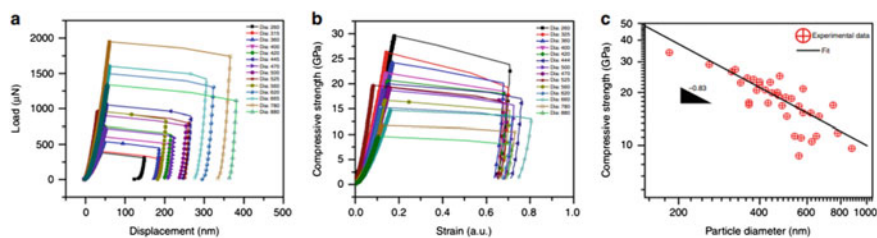


Fig. 12 **a** Load–displacement curves for different particle sizes of NPs. **b** Stress–strain curves demonstrate that the strength increases with decreasing particle diameter. **c** Compressive strength as a function of particle diameter [150]

4.4 Thermal Properties

Water, phase change materials, oil and ethylene glycol are typical heat transfer fluids, and they are mostly used as cooling fluid in many thermal engineering applications. In general, the thermal conductivity of a standard heat transfer fluid is lower than <1 W/mK [151]. Among them, water offers the highest value of thermal conductivity (0.613 W/mK at 303 K). This is still not comparable to the value that metal NPs can offer. Ag, Al, Cu, Fe and Au NPs can offer the high thermal conductivity of

429 W/mK at 300 K, 237 W/mK at 273 K, 401 W/mK at 273–373 K, 80.4 W/mK at 273–373 K and 318 W/mK at 273–373, respectively [152, 153]. For this reason, the heat transfer fluid, which is known as nanofluid (a combination of traditional heat transfer fluids with metallic NPs that have size less than 100 nm and at very low concentration of less than 1%), has attracted huge attention to researchers in the past decade [154]. It has been reported that thermal conductivity of water can be improved by 54% through an addition of 0.1% weight of 20 nm Ag NPs [152]. Many reports agree that size, shape and volume fraction of NPs can directly affect the thermal conductivities of typical heat fluids [154, 155]. In the case of Ag, the thermal conductivity of nanofluids increases with decreasing size and increasing the concentration of nanoparticles [156].

For given volume fraction and temperature, the thermal conductivity of nanofluid containing rectangular nanoparticles was higher than those with NPs in spherical shape. Additionally, metal nanoparticles can be added into polymers, such as epoxy, to enhance thermal conductivity and to maintain electrical insulation below percolation threshold. Compared with the electrical properties in metal–polymer composites, thermal transport does not show any dramatic increase [157]. However, similar trend for metal/heat transfer fluids, it has been reported that Ni NPs with the size of 40 nm show higher thermal conductivities of 0.37 W/mK due to its wider-spread aggregation structures in epoxy compared to those larger Ni NPs with size of 70 nm (0.31 W/mK) [158].

5 Conclusion

Bottom-up techniques are more precise than top-down techniques in controlling particle size distribution. Controlling the component concentration, reaction time and temperature can be achieved with different particle sizes and shapes, or NPs. Despite the fact that these growth conditions are extremely sensitive to process variables, limiting the variation of NP morphologies and structures, top-down methods, on the other hand, have advantages over bottom-up methods, such as simple production, the use of non-organic precursors and the high potential for large-scale production with high yields. The size distribution can be controlled via the evaporation rate, system pressure or system geometry. Although many researchers have successfully prepared various types of NPs using various techniques, the precise information of the parameter conditions of each technique that allow to optimize the designed size and shape of various types of NPs is unclear and necessitates additional research for an accurate reproduction process. Mass production could be taken into consideration for further development of the metal NPs. The long-term stability of NPs and their toxicity, especially in biotechnologies, are still unclear. An intensive study must be conducted to investigate the composition, morphology, size, shape, structure and side effects of metal NPs for diverse applications in the fields of magnetic, thermal, optical, etc.

Acknowledgements This work was supported by the Leverhulme Trust Early Career Fellowship (ECF-2021-657) and Nottingham Research Fellowship (A7X164).

Conflicts of Interest There are no conflicts to declare.

References

1. Haritha VS, Balan M, Hosson JTM, Krishnan G (2020) *Nanoscale Adv* 2:9
2. Krishnan G, Kooi BJ, Palasantzas G, Pivak Y, Dam B (2010) *J Appl Phys* 107:5
3. Liang L, Wang F, Rong M, Wang Z, Yang S, Wang J, Zhou H (2020) *J Mater Sci Chem Eng* 8:12
4. Munoz JE, Cervantes J, Esparza R, Rosas G (2007) *J Nano Res* 9:5
5. Zarrouk T, Nouari M, Salhi JE, Makich H, Salhi M, Atlati S, Salhi N (2022) *Int J Adv Manuf Technol* 119
6. Dercz G, Matula I, Zubko M, Liberska A (2016) *Acta Physica Polonoca A* 130:4.7
7. Pradeep NB, Rajath Hegde MM, Manjunath Patel GC, Giasin K, Pimenov DY, Wojciechowski S (2022) *J Mater Res Technol* 16
8. Hu X, Sun Z, Zhang C, Wang X, Wu K (2018) *J Magnes Alloy* 6:2
9. El-Eskandarany MS, Al-Hazza A, Al-Hajji LA, Ali N, Al-Duweesh AA, Banyan M, Al-Ajmi F (2021) *Nanomaterials (Basel)* 11:10
10. Oleszak D, Pawlyta M, Pikula T (2021) *Materials (Basel)* 14:24
11. Toozandehjani M, Matori KA, Ostovan F, Abdul Aziz S, Mamat MS (2017) *Materials* 10:11
12. Piras CC, Fernández-Prieto S, De Borggraeve WM (2019) *Nanoscale Adv* 1:3
13. Lopes WA, Jaeger HM, (2001) *Nature* 414.
14. Colson P, Henrist C, Cloots R (2013) *J Nanomater* 2013:948510
15. Kothari R, Beaulieu MR, Hendricks NR, Li S, Watkins JJ (2017) *Chem Mater* 29:9
16. Kim DE, Sung IH (2013) In: Wang QJ, Chung YW (eds) *Encyclopedia of Tribology*. Springer, Boston, MA
17. Lipomi DJ, Martinez RV, Cademartiri L, Whitesides GM In: Matyjaszewski K, Moller M (eds) *Polymer science: a comprehensive reference*. Elsevier BV, Amsterdam, NL
18. Paivanranta B, Langner A, Kirk E, David C, Ekinici Y (2011) *Nanotechnology* 22:37
19. Auzelyte V, Dais C, Farquet P, Gruetzmacher D, Heyderman L, Luo F, Olliges S, Padeste C, Sahoo P, Thomson T, Turchanin A, David C, Solak H (2009) *J Micro/Nanolithogr* 8:2
20. Vala M, Homola J (2014) *Opt Express* 22:15
21. Kim P, David E, Raboin L, Ribbe AE, Russell TP, Hoagland DA (2013) *Microsc Microanal* 19:6
22. Luo S, Hoff BH, Maier SA, De-Mello JC (2021) *Adv Sci* 8:24
23. Wu D, Rajput SN, Luo X (2016) *Curr Nanosci* 12:6
24. Leggett GJ (2011) *ACS Nano* 5:3
25. Fan P, Gao J, Mao H, Geng Y, Yan Y, Wang Y, Goel S, Luo X (2022) *Micromachines* 13:2
26. Savale PA, (2016) *Arch Appl Sci Res* 8
27. Grillo F, Van Bui H, Moulijn JA, Kreutzer MT, Van-Ommen JR (2017) *J Phys Chem Lett* 8:5
28. Kuwata N, Kawamura J, Toribami K, Hattori T, Sata N (2004) Thin-film lithium-ion battery with amorphous solid electrolyte fabricated by pulsed laser deposition. *Electrochem Commun* 6:4
29. Saunders SRJ, Nicholls JR (1996) In: Cahn RW, Haasen P (eds) *Physical metallurgy*, 4th edn.. North-Holland, Oxford, UK
30. Kerdcharoen T, Wongchoosuk C (2013) In: Jaaniso R, Tan OK (eds) *Semiconductor gas sensors*. Woodhead Publishing
31. Kozhemyakin GN, Kiiko SA, Bryl OE (2019) *Crystallogr Rep* 64:3

32. Luttge R (2011) In: Luttge R (eds) *Microfabrication for industrial applications*. William Andrew Publishing, Boston, US
33. Baptista A, Silva FJG, Porteiro J, Miguez JL, Pinto G (2018) *Coatings* 8:11
34. Suryanarayana C, Prabhu B (2007) In: Koch CC (eds) *Nanostructured materials*, 2nd edn. William Andrew Publishing, Norwich, NY
35. Shahidi S, Moazzenchi B, Ghoranneviss M (2015) *Eur Phys J Appl Phys* 71:3
36. Yin Y, Lan C, Hu S, Li C (2018) *J Alloys Comp* 739
37. Pandey PA, Bell GR, Rourke JP, Sanchez AM, Elkin MD, Hickey BJ, Wilson NR (2011) *Small* 7:22
38. Fernandez-Arias M, Zimbone M, Boutinguiza M, Del-Val J, Riveiro A, Privitera V, Grimaldi MG, Pou J (2019) *Coatings* 9:9
39. Donnelly T, O'Connell G, Lunney JG (2022) *Nanomaterials* 10:11
40. Khalily MA, Yurderi M, Haider A, Bulut A, Patil B, Zahmakiran M, Uyar T (2018) *ACS Appl Mater Interfaces* 10:31
41. Moret JLT, Griffiths MBE, Frijns JEBM, Terpstra BE, Wolterbeek HT, Barry ST, Denkova AG, Ommen JRV (2020) *J Vac Sci Technol A* 38:2
42. Kumar G, Jagirdar Rao V (2013) *Int J Nanotechnol Appl* 3:1
43. Sun G, Ye G, Wang K, Lou M, Jia X, Xu F, Ye Z (2020) *ACS Omega* 5:13
44. Ceylan A, Rumaiz AK, Shah SI (2007) *J Appl Phys* 101:9
45. Gracia-Pinilla M, Martinez E, Vidaurri GS, Perez-Tijerina E (2009) *Nanoscale Res Lett* 5:1
46. Silva LG, Solis-Pomar F, Gutierrez-Lazos CD, Melendrez MF, Martinez E, Fundora A, Perez-Tijerina E (2014). *J Nanomater* 2014:643967
47. Ward MB, Brydson R, Cochrane RF (2006) *J Physics: Conf Ser* 26:296
48. Alexandrescu R, Morjan I, Dumitrache F, Scarisoreanu M, Soare I, Fleaca C, Birjega R, Popovici E, Gavrilă L, Prodan G, Ciupina V, Filoti G, Kuncser V, Vekas L (2008) *Int J Photoenergy* 2008:604181
49. Bendre K, Bhat MP, Lee KH, Altalhi T, Ayad Alruqi M, Kurkuri M (2022) *Mater Today Adv* 13:100205
50. Spreafico C, Russo D, Degl-Innocenti R (2022) *J Intell Manuf* 33:2
51. Jamkhande PG, Ghule NW, Bamer AH, Kalaskar MG (2019) *J Drug Deliv Sci Technol* 53:101174
52. Esposito S (2019) *Materials (Basel)* 12:4
53. Modan EM, Plaiasu AG (2020) The annals of "Dunarea de Jos" University of Galati, Fascicle IX. *Metall Mater Sci* 43:1. Accessed 15 Mar 2020
54. Bokov D, Turki Jalil A, Chupradit S, Suksatan W, Javed Ansari M, Shewael IH, Valiev GH, Kianfar E (2021) *Adv Mater Sci Eng* 2021:5102014
55. Danks AE, Hall SR, Schnepf Z (2016) *Mater Horiz* 3:2
56. Mahmud NA, Habiballah AS, Affandi NSM, Osman N, Jani AMM (2018) *AIP Conf Proc* 2031:1
57. Jameel ZN (2017) *Energy Procedia* 119
58. Hamada Y, Nishi M, Shimotsuma Y, Miura K, Hirao K (2011) *IOP Conf Ser: Mater Sci Eng* 8:3
59. Ligabue ML, Terzi F, Zanardi C, Lusvardi G (2019) *J Mater Sci* 54:13
60. Gondal MA, Rashid SG, Dastageer MA, Zubair SM, Ali MA, Lienhard JH, McKinley GH, Varanasi KK (2013) *IEEE Photonics J* 5:3
61. Ingale SV, Wagh PB, Bandyopadhyay D, Singh IK, Tewari R, Gupta SC (2015) *IOP Conf Ser: Mater Sci Eng* 73:1
62. Ahlawat DS, Kumari, R, Rachna, Yadav I (2014) *Int J Nanosci* 13:1
63. Mohindru JJ, Garg UK (2017) *Int J Theor Appl Sci* 9:2
64. Panigrahi S, Kundu S, Ghosh S, Nath S, Pal T (2004) *J Nanopart Res* 6:4
65. Piszczek P, Radtke A. (2018) In: Seehra MS, Bristow AD (eds) *Noble and precious metals—properties, nanoscale effects and applications*. IntechOpen, London, UK. Accessed 20 Dec 2017

66. Xia L (2021) In: Osaka A, Narayan R (eds) *Advanced ceramic materials: bioceramics*. Elsevier, Osaka, JP
67. Chew CKT (2016) *Chemical vapour deposition of gold nanoparticles and metal oxide composites*. Dissertation, University College London
68. Ng JJ, Leong KH, Sim LC, Oh WD, Dai C, Saravanan P (2020) In: Abdeltif A, Assadi AA, Nguyen-Tri P, Nguyen TA, Rtimi S (eds) *Micro and nano technol: nanomaterials for air remediation*. Elsevier, Amsterdam, NL
69. Dunne PW, Munn AS, Starkey CL, Huddle TA, Lester EH (2015) *Philos Trans A Math Phys Eng Sci* 373:2057
70. Qiu J, Li Y, Jia Y (2021) In: Qiu J, Li Y, Jia, Y (eds) *Persistent phosphors from fundamentals to applications: synthesis method*. Woodhead Publishing, Oxford, UK
71. Tipayawat P, Phromviyo N, Boueroy P, Chompoosor A (2016) *Peer J* 4
72. Liu Y, Yang L, Shen Y (2018) *J Mater Res* 33:18
73. Murugan S, Grace A (2012) *J Nano Res* 18:1
74. Lozhkomoev AS, Kazantsev SO, Pervikov AV (2020) *AIP Conf Proc* 2310:1
75. Cored J, Garcia-Ortiz A, Iborra S, Climent MJ, Liu L, Chuang CH, Chan TS, Escudero C, Concepcion P, Corma A (2019) *J Am Chem Soc* 141:49
76. Parveen K, Banse V, Ledwani L (2016) *AIP Conf Proc* 1724:1
77. Boroumand Moghaddam A, Namvar F, Moniri M, Md Tahir P, Azizi S, Mohamad R (2015) *Molecules* 20:9
78. Roychoudhury A (2020) *Indian J Pham Biol Res* 8:3
79. Sun Y, Wang Q, Chen J, Liu L, Ding L, Shen M, Li J, Han B, Duan Y (2017) *Theranostics* 7:18
80. Ijaz I, Gilani E, Nazir A, Bukhari A (2020) *Green Chem Lett Rev* 13:3
81. Zhang D, Ma XI, Gu Y, Huang H, Zhang G (2020) *Front Chem* 8
82. AbdelRahim K, Mahmoud SY, Ali AM, Almaary KS, Mustafa AEZMA, Husseiny SM (2017) *Saudi. J Biol Sci* 24:1
83. Guilger-Casagrande M, Lima RD (2019) *Front Bioeng Biotechnol* 7:287
84. AlNadhari S, Al-Enazi NM, Alshehri F, Ameen F (2021) *Environ Res* 194:110672
85. Chandran SP, Chaudhary M, Pasricha R, Ahmad A, Sastry M (2006) *Biotechnol Prog* 22:2
86. Rautela A, Rani J, Debnath M (2019) *J Anal Sci Technol* 10:1
87. Yulizar Y, Utari T, Ariyanta HA, Maulina D (2017) *J Nanomater* 2017:3079636
88. Mali SC, Dhaka A, Githala CK, Trivedi R (2020) *Biotechnol Rep* 27:e00518
89. Amjad R, Mubeen B, Ali SS, Imam SS, Alshehri S, Ghoneim MM, Alzarea SI, Rasoo R, Ullah I, Nadeem MS, Kazmi I (2021) *Polymers (Basel)* 13:24
90. Wu S, Rajeshkumar S, Madasamy M, Mahendran V (2020) *Artif Cells Nanomed B* 48:1
91. Varaprasad T, Govindh B, Venkateswara Rao B (2017) *Int J ChemTech Res* 10:9
92. Sunkar S, Nachiyar CV (2012) *Asian Pac J Trop Biomed* 2:12
93. Du L, Jiang H, Liu X, Wang E (2007) *Electro Comm* 9:5
94. Mikheenko IP, Bennett JA, Omajali JB, Walker M, Johnson DB, Grail BM, Wong-Pascua D, Moseley JD, Macaskie LE (2022) *Appl Catal B: Environ* 306:121059
95. Ahghari MR, Soltaninejad V, Maleki A (2020) *Sci Rep* 10:1
96. Raliya R, Tarafdar JC (2014) *Int Nano Lett* 4:1
97. Li Y, Li Y, Li Q, Fan X, Gao J, Luo Y (2016) *J Chem* 2016:2781347
98. Pimprikar PS, Joshi SS, Kumar AR, Zinjarde SS, Kulkarni SK (2009) *Colloids Surf B: Biointerfaces* 74:1
99. Tian X, He W, Cui J, Zhang X, Zhou W, Yan S, Sun X, Han X, Han S, Yue Y (2010) *J Colloid Interface Sci* 343:1
100. Arya A, Gupta K, Chundawat TS, Vaya D (2018) *Bioinorg Chem Appl* 2018:7879403
101. Yılmaz Ozturk B, Yenice Gursu B, Dag I (2020) *Process Biochem* 89
102. Senapati S, Syed A, Moez S, Kumar A, Ahmad A (2012) *Mater Lett* 79
103. Mourdikoudis S, Pallares RM, Thanh NTK (2018) *Nanoscale* 10:27
104. Tiede K, Boxall ABA, Tear SP, Lewis J, David H, Hasselvo M (2008) *Food Addit Contam: Part A* 25:7

105. Khan I, Saeed K, Khan I (2019) *Arabian J Chem* 12:7
106. Lubenchenko AV, Batrakov AA, Pavolotsky AB, Lubenchenko OI, Ivanov DA (2018) *Appl Surf Sci* 427
107. Baer DR, Engelhard MH (2010) *J Electron Spectrosc Relat Phenom* 178–179
108. Yano J, Yachandra VK (2009) *Photosynth Res* 102:2–3
109. Terzano R, Denecke MA, Falkenberg G, Miller B, Paterson D, Janssens K (2019) *Pure Appl Chem* 91:6
110. Penner-Hahn JE, X-ray absorption spectroscopy. In *eLS*
111. Manjumeena R (2018) In: Tiwari A (eds) *Handbook of antimicrobial coatings*. Elsevier
112. Faghihzadeh F, Anaya NM, Schiffman LA, Oyanedel-Craver V (2016) *Nanotechnol Environ Eng* 1:1
113. Venkatesh N (2018) *Biomed J Sci Technol* 4
114. Shnoudeh AJ, Hamad I, Abdo RW, Qadumii L, Jaber AY, Surchi HS, Alkelany SZ (2019) In: Tekade RK (eds) *Biomaterials and bionanotechnology*. Academic Press
115. Zavasnik J, Sestan A, Shvalya V (2021) In: Milacic R, Scancar J, Goenaga-Infante H, Vidmar J (eds) *Comprehensive analytical chemistry*. Elsevier, Amsterdam, NL
116. Eaton P, Quaresma P, Soares C, Neves C, De-Almeida MP, Pereira E, West P (2017) *Ultramicroscopy* 182
117. Malm AV, Corbett JCW (2019) *Sci Rep* 9:1
118. Griffiths D, Hole WBP, Smith J, Malloy A, Carr B (2011) *NSTI-Nanotech 1*
119. Clogston JD, Patri AK (2011) In: McNeil S (eds) *Characterization of nanoparticles intended for drug delivery*. Humana Press, Maryland, USA
120. Nanocomposix, Zeta Potential Measurements (2022) <https://nanocomposix.com/pages/zeta-potential-measurements>
121. Bonnin EA, Rizzoli SO (2020) *Front Behav Neurosci* 14
122. Wang C, Gao X, Chen Z, Chen Y, Chen H (2017) *Polymers* 9:12
123. Din M, Arshad F, Hussain Z, Mukhtar M (2017) *Nanoscale Res Lett* 12
124. Linkov P, Artemyev M, Efimov AE, Nabiev I (2013) *Nanoscale* 5:19
125. Choudhary OP, Choudhary P (2017) *Int J Curr Microbiol Appl Sci* 6
126. Smith DJ (2015) *Nanocharacterisation*. The Royal Society of Chemistry
127. Chiriaco M, Bianco M, Nigro A, Primiceri E, Ferrara F, Romano A, Quattrini A, Furlan R, Arima V, Maruccio G (2018) *Sensors* 18:3175
128. Lim J, Yeap SP, Che HX, Low SC (2013) *Nanoscale Res Lett* 8:1
129. Grunder Y, Lucas C (2016) *Nano Energy* 29:1
130. Baer DR (2022) *J Vac Sci Technol* 38:3
131. San-Miguel A (2005) *Acta Crystallogr Sec A* 61.
132. Bak SM, Lin R, Yu X, Yang XQ (2018) *NPG Asia Mater* 10
133. Thermoscientific, Advantages of a Fourier Transform Infrared Spectrometer (Technical Note). <https://www.thermoscientific.com/content/dam/tfs/ATG/CAD/CAD%20Documents/Application%20%26%20Technical%20Notes/Molecular%20Spectroscopy/FTIR/FTIR%20Spectrometers/TN50674-E-0215M-FT-IR-Advantages.pdf>
134. Baer DR, Engelhard MH, Johnson GE, Laskin J, Lai J, Mueller K, Munusamy P, Thevuthasan S, Wang H, Washnton N, Elder A, Baisch BL, Karakoti A, Kuchibhatla SVNT, Moon D (2013) *J Vac Sci Technol A* 31:5
135. Khandel P, Shahi KS (2016) *Int J Nanomater Biostruc* 6:1
136. Fratoddi I, Matassa R, Fontana L, Venditti I, Familiari G, Battocchio C, Magnano E, Nappini S, Leahu G, Belardini A, Li Voti R, Sibilia C (2017) *J Phys Chem C* 121:33
137. Zhu S, Zhou W (2010) *J Nanomater* 2010:562035
138. Sau TK, Rogach AL, Jackel F, Klar TA, Feldmann J (2010) *Adv Mater* 22:16
139. Murphy CJ, Gole AM, Hunyadi SE, Stone JW, Sisco PN, Alkilany A, Kinard BE, Hankins P (2008) *Chem Comm* 5
140. Mulvaney P (1996) *Optical properties of metal clusters* By U. Kreibig, M. Vollmer, Springer Series in Materials Science, Advanced Materials. Wiley, Hardcover, DM
141. Issa B, Obaidat IM, Albiss BA, Haik Y (2013) *Int J Mol Sci* 14:11

142. Diaz C, Valenzuela ML, Laguna-Bercero MA, Orera A, Bobadilla D, Abarca S, Pena O (2017) RSC Adv 7:44
143. Sani A, Cao C, Cui D (2021) Biochem Biophys Rep 26
144. Leon Felix L, Sanz B, Sebastian V, Torres TE, Sousa MH, Coaquira JAH, Ibarra MR, Goya GF (2019) Sci Rep 9:1
145. Luo X, Morrin A, Killard AJ, Smyth MR (2006) Electroanalysis 18:4
146. Hussain F, Hojjati M, Okamoto M, Gorga RE (2006) J Comp Mater 40:17
147. Maharaj D, Bhushan B (2014) Beilstein J Nanotechnol 5
148. Guo D, Li J, Chang L, Luo J (2013) Langmuir 29:23
149. Ritter C, Heyde M, Schwarz UD, Rademann K (2002) Langmuir 18:21
150. Sharma A, Hickman J, Gazit N, Rabkin E, Mishin Y (2018) Nat Comm 9:1
151. Mbambo MC, Khamlich S, Khamliche T, Moodley MK, Kaviyarasu K, Madiba IG, Madito MJ, Khenfouch M, Kennedy J, Henini M, Manikandan E, Maaza M (2020) Sci Rep 10:1
152. Iyahraja S, Rajadurai JS (2015) AIP Adv 5:5
153. Farid N, Sedigheh A (2017) J Adv Mater Proc 5:2
154. Liu M, Ma Y, Wu H, Wang RY (2015) ACS Nano 9:2
155. Navarrete N, Gimeno-Furio A, Mondragon R, Hernandez L, Cabedo L, Cordoncillo E, Julia JE (2017) Sci Rep 7:1
156. Warriar P, Teja A (2011) Nanoscale Res Lett 6:1
157. Guoqing Z, Yanping X, Hui W, Yu T, Guoliang T, Shantung T, Haiping W (2009) J Comp Mater 44:8
158. Li X, Park W, Chen YP, Ruan X (2013) J Heat Transfer 139:2